On the Minimum Ignition Energy and its transition in the localised forced ignition of turbulent homogeneous mixtures

Charles Turquand d'Auzay[a,*], Vassilios Papapostolou[a], Samer F. Ahmed[b], Nilanjan Chakraborty[a]

[a] *School of Engineering, Newcastle University, Newcastle-Upon-Tyne NE1 7RU, United Kingdom*
[b] *Thermofluids Group, Department of Mechanical and Industrial Engineering, College of Engineering, Qatar University, P.O. Box 2713, Doha, Qatar*

Abstract

The minimum energy requirements for ensuring *(i)* just successful ignition and *(ii)* successful self-sustained flame propagation without the assistance of an external energy source following a successful ignition event have been analysed for the forced ignition of a homogeneous stoichiometric methane-air mixture under a wide range of turbulence intensities using three-dimensional Direct Numerical Simulation (DNS) data. It has been found that the minimum energy needed for successful ignition is also sufficient to ensure self-sustained flame propagation for small turbulence intensities. However, for large turbulence intensities, the minimum energy for ensuring self-sustained flame propagation can be considerably greater than the minimum energy needed just to successfully ignite the mixture. At low turbulence intensities, the thermal runaway has been obtained for the minimum ignition energy after the end of the energy deposition indicating an autoignition. For larger energy inputs and turbulence intensity, the thermal runaway was obtained during the energy deposition period. It has been found that the minimum energy requirements for ignition and self-sustained flame propagation increase with increasing turbulence intensity but a transition in this behaviour has been observed. There is a critical turbulence intensity such that the increase in the energy demand is significantly more rapid above the critical value than that for turbulence intensities smaller than the critical value. This has been found to be qualitatively consistent with previous experimental findings. The stochastic nature of the ignition event has been demonstrated by considering different realisations of statistically similar turbulent flow fields. The conditions giving rise to a successful ignition have been identified by a detailed analysis of the energy budget. A scaling analysis has been performed for the critical condition for ensuring self-sustained flame propagation and the insights gained from this analysis have been utilised to explain the physical mechanisms behind the transition of the minimum ignition energy.

Keywords: Minimum ignition energy, localised forced ignition, homogeneous mixture, premixed flame, Direct Numerical Simulation

*Corresponding author
Email address: nct92@ncl.ac.uk (Charles Turquand d'Auzay)

1. Introduction

Localised forced ignition (e.g. spark or laser ignition) of homogeneous mixtures plays a pivotal role in the effective utilisation of fuel in Spark Ignition (SI) engines and industrial gas turbines. Because of its fundamental importance, the localised forced ignition has been extensively analysed by various researchers by analytical [1–3], experimental [4–17] and computational [18–26] methodologies. The ignition characteristics in quiescent homogeneous gaseous mixtures due to a point ignition source have been investigated by Espi and Liñàn [1, 2]. Champion and Deshaies [3] developed analytical tools to address flame initiation whose predictions compare favourably with experiments. Although these analytical studies [1–3] were conducted for laminar conditions, they provided fundamental physical insights even for turbulent conditions. Lefebvre and co-workers [4–7] carried out an extensive experimental analysis on propane-air, iso-octane, diesel oil and heavy fuel oil and demonstrated that the critical radius increases with increasing turbulence intensity and with decreasing equivalence ratio. This indicates that more energy is needed to ignite fuel-lean and fuel-rich mixtures in comparison to the stoichiometric mixture and this tendency becomes more prevalent for high turbulence intensities. Huang *et al.* [8] and Shy *et al.* [9] analysed the minimum ignition energy (MIE) under homogeneous isotropic forced turbulence for different equivalence ratio values of homogeneous methane-air mixtures and different turbulence intensities u'/s_l^0 (where u' is the root-mean-square (RMS) value of turbulent velocity fluctuations and s_l^0 is the unstrained laminar burning velocity). A transition in the increase of MIE with an increase of turbulence intensity has been observed at a critical value u_c'/s_l^0 such that the MIE requirement for $u'/s_l^0 \geqslant u_c'/s_l^0$ is significantly higher than that for $u'/s_l^0 \leqslant u_c'/s_l^0$, and this has been justified based on scaling arguments by Shy *et al.* [9]. Shy and co-workers also investigated the MIE transition dependence on various parameters including spark gap distance, equivalence ratio, fuel type and pressure [8, 9, 13, 15–17]. Using laser ignition in isotropic homogeneous decaying turbulence, a similar transition has been obtained for lean methane-air mixtures by Cardin *et al.* [11, 12]. These two experimental results show that the transition occurrence is independent of the ignition system (spark or laser) and fuel considered and that a common criterion can be found to characterize the transition, i.e. Ka ~ 10. However, some differences in the critical turbulence intensity and MIE dependence on the turbulence intensity were highlighted by Cardin *et al.* [11]. These differences have been attributed to variations in the ignition apparatus, experimental set-up and integral length scale of turbulence between the experiments.

It has recently become possible to carry out three-dimensional Direct Numerical Simulations (DNS) of localised forced ignition of homogeneous mixtures to analyse the early stages of premixed flame kernel development [22–26]. The detrimental effects of turbulence intensity have also been numerically confirmed using DNS [22, 26]. Patel and Chakraborty [26] analysed the effects of the energy deposition characteristic width, duration, total energy and turbulence intensity for different equivalence ratios in homogeneous mixtures, and computationally confirmed the findings from Refs. [4–7, 18] in a qualitative sense. Interested readers are

referred to Refs. [27, 28] for further review of the literature on localised forced ignition of both homogeneous and inhomogeneous mixtures.

Although the existing numerical investigations [19–26, 29] provided significant physical insights into localised forced ignition of homogeneous mixtures, the transition of MIE between small and high values of u'/s_l^0 reported experimentally by Shy and co-workers [8, 9, 13, 15–17] and Cardin *et al.* [11, 12] has not been computationally analysed to the best of the knowledge of the authors of this paper. In the present analysis, three-dimensional simple chemistry DNS of localised forced ignition of homogeneous stoichiometric methane-air mixtures under decaying homogeneous isotropic turbulence have been utilised to evaluate the minimum energy leading either to *(i)* at least a successful ignition or to *(ii)* a successful ignition followed by a self-sustained combustion once the ignitor has been switched off. The main objectives of this work are thus to **(1)** analyse the variation of the MIE requirements for successful ignition and for subsequent flame propagation for different initial intensities of homogeneous isotropic turbulence using DNS and to **(2)** explain the transition of MIE between small and large values of u'/s_l^0 based on the physical insights gained from DNS data.

The rest of the paper will be organised as follows, the mathematical background and numerical implementation will be presented in the next two sections. Following that, the results will be presented and subsequently discussed. The main findings and the conclusions drawn from them will be summarised in the final section.

2. Mathematical background

The wide range of initial turbulence intensities investigated here, added to the fact that multiple simulations are needed to identify the MIE and its statistics accurately, means that the current study is computationally intensive. Moreover, the present flame-turbulence interaction is not significantly influenced by the choice of the chemical mechanism. Thus, a single-step chemical mechanism has been used, that is given by,

$$\text{Fuel} + \text{s} \cdot \text{Oxidiser} \rightarrow (1 + \text{s})\text{Products}, \tag{1}$$

where s indicates the mass of oxygen consumed per unit mass of fuel consumption under stoichiometric conditions. The fuel reaction rate is given by an Arrhenius type expression [26, 30–34], which reads,

$$\dot{\omega}_f = -\rho B^* Y_f Y_o \exp\left[\frac{-\beta(1-T)}{1-\alpha(1-T)}\right], \tag{2}$$

where ρ is the gas density, Y_f and Y_o are the fuel and oxidiser mass fraction respectively. The dimensionless temperature is defined as $T = (\hat{T} - T_0)/(T_{\text{ad}} - T_0)$ where $\hat{T}$, T_0 and T_{ad} are the dimensional instantaneous, reactants and stoichiometric adiabatic flame temperatures respectively. In Eq. 2, β is the Zel'dovich number,

defined as $\beta = \left(T_{\rm ac}\left[T_{\rm ad} - T_0\right]\right)/T_{\rm ad}^2$, where $T_{\rm ac}$ is the activation temperature, $\alpha = \left(T_{\rm ad} - T_0\right)/T_{\rm ad}$ is a heat release parameter and B^* is the normalised pre-exponential factor. The extent of the completion of the chemical reaction can be quantified by a reaction progress variable c rising monotonically from 0 in the reactants to 1 in the products, defined as $c = (Y_{f,u} - Y_f)/(Y_{f,u} - Y_{f,b})$ [26, 30] where $Y_{f,u}$ and $Y_{f,b}$ are the mass fractions of fuel in the reactants and products respectively.

It is worth mentioning here that several previous DNS studies have shown the validity of a single-step chemical mechanism compared to detailed chemistry. It was found that the statistical behaviour of the reaction rate [35, 36], flame propagation [35, 37], and scalar gradient statistics [36, 38, 39] are adequately captured by a single-step chemical mechanism. A recent analysis by Haghiri *et al.* [40] discussed the ability of simple chemistry to match important physical parameters such as laminar flame speed, flame thickness and temperature ratio across the flame. Thus, single-step chemistry is usually preferred over detailed mechanisms when an extensive parametric analysis is involved, as in the case of the current work which required tens of simulations.

Furthermore, the success of ignition and the occurrence of self-sustained flame propagation are dependent on the competition between the heat release rate due to chemical reactions and the heat transfer from the hot gas kernel, and these mechanisms are correctly captured by a single-step chemistry. In this regard, it is worth highlighting that a large number of single-step chemistry based analytical studies [1–3, 41] offered fundamental physical insights into localised forced ignition. Finally, findings on localised forced ignition by previous simple chemistry DNS studies [42–44] have been found to be qualitatively consistent with those obtained from detailed chemistry simulations [32, 45, 46].

The effects of the localised forced ignition are accounted for by the addition of a source term to the energy conservation equation, q''' [26, 30–34],

$$\frac{\partial}{\partial t}\rho E \underbrace{+\frac{\partial}{\partial x_i}\rho u_i E}_{-C_1} = \underbrace{-\frac{\partial}{\partial x_i}u_i P}_{P_1} \underbrace{+\frac{\partial}{\partial x_i}\tau_{ij}u_j}_{D_1} \underbrace{+\dot{\omega}_T}_{P_2} \underbrace{+\frac{\partial}{\partial x_k}\left[\lambda\frac{\partial \hat{T}}{\partial x_i}\right]}_{D_2} \underbrace{-\frac{\partial}{\partial x_i}\rho\sum_{k=1}^{N} h_{s,k}Y_k V_{k,i}}_{D_3} \underbrace{+q'''}_{P_3}, \tag{3}$$

where E is the specific stagnation internal energy ($E = C_v\hat{T} + u_i u_i/2$, where C_v is the heat capacity at constant volume), u_i is the i-th velocity component, $h_{s,k}$ is the specific enthalpy of the k-th species, P is the pressure, $\dot{\omega}_T = |\dot{\omega}_f| H_\phi$ is the heat release due to combustion (where $H_\phi = \left[\left(T_{\rm ad} - T_0\right) C_p\right] / \left[Y_{f,u} - Y_{f,b}\right]$ is the heat release per unit mass of fuel consumption) and τ_{ij} is the viscous shear stress tensor. The species are considered to be perfect gases with constant and identical properties, i.e. heat capacities at constant pressure and volume (C_p and C_v), viscosity (μ), thermal conductivity (λ) and density weighted mass diffusivity (ρD). These assumptions lead to $\rho\sum_{k=1}^{N} h_{s,k}Y_k V_{k,i} = C_p\left(T - T_0\right)\sum_{k=1}^{N} Y_k V_{k,i} = 0$. The source term q''' is taken to follow a Gaussian distribution in the radial direction from the ignition centre [1, 2, 26, 30–34] and is

expressed as,

$$q''' = A_{sp} \exp\left(-r^2/2R_{sp}^2\right), \tag{4}$$

where r is the distance from the ignitor centre and R_{sp} is the characteristic width of energy deposition. The constant A_{sp} is determined by a volume integration leading to the total ignition power $\dot{Q}$ given by,

$$\dot{Q} = \int_V q''' \, \mathrm{d}V = a_{sp}\rho_0 C_p \tau T_0 \left(\frac{4}{3}\pi\delta_z^3\right)\left[\frac{\mathcal{H}(t) - \mathcal{H}(t - t_{sp})}{t_{sp}}\right], \tag{5}$$

where a_{sp} is a parameter determining the total energy deposited by the ignitor [26, 30–34], $\tau = (T_{\mathrm{ad}} - T_0)/T_0$ is the heat release parameter, δ_z is the Zel'dovich flame thickness ($\delta_z = D_0/s_l^0$ where D_0 is the reactants mass diffusivity) and $\mathcal{H}(t)$ and $\mathcal{H}(t - t_{sp})$ are Heaviside functions that ensure that the ignitor is only active until $t = t_{sp}$. The energy deposition duration t_{sp} is expressed as $t_{sp} = b_{sp}t_f$ where b_{sp} is the energy deposition parameter and $t_f = \delta_z/s_l^0$ is a characteristic chemical time scale. The suggested range for optimal duration of energy deposition is $0.2 \leqslant b_{sp} \leqslant 0.4$ [47]. For a shorter duration, strong shock waves that dissipate energy can be formed, and for a longer one, the temperature is wastefully dissipated outside of the energy deposition region.

The choice of a spherical shape for the ignitor was driven by the choice to have an isotropic energy deposition region following previous analysis [1, 2, 31, 32, 44, 48] with the aim of eliminating the potential effects of ignitor geometry on the MIE. In order to confirm that the energy deposition profile does not alter the qualitative nature of the results, a limited number of simulations have been carried out using a cylindrical profile of energy deposition using identical input energy and duration parameters as in the spherical case. It has been found that both the flame propagation and the MIE behaviour for the cylindrical energy deposition profile were qualitatively similar to that of the spherical one.

Here, the ignition power has been modified whilst the energy deposition duration and width are kept constant to find the minimum energy levels leading to either of the two following phenomena :

1. A successful *ignition* refers to a situation where the maximum temperature surpasses the adiabatic flame temperature during or after the energy deposition period regardless of subsequent flame behaviour. If the maximum temperature does not reach the adiabatic flame temperature, it is referred to as a misfire in the following discussion.
2. A successful *self-sustained propagation* is obtained when the flame kernel burns without the aid of the ignitor after a successful ignition. It is determined by evaluating the temporal evolution of the burned gas volume, that is, if the temporal derivative is positive at the end of the simulation time or when the kernel leaves the computational domain, a successful self-sustained propagation is obtained, otherwise it is considered failed or quenched.

Note that a successful ignition does not necessarily give rise to a successful self-sustained combustion. As discussed and demonstrated later, as the turbulence intensity increases, the energy required to simply ignite the mixture differs from the energy required to obtain self-sustained combustion under the same turbulent conditions. It was thus deemed necessary to investigate both events. Thus, finding the MIE consists of finding the values of a_{sp} which are sufficient to either *(i)* produce at least a successful ignition or *(ii)* ensure a successful ignition and the subsequent flame propagation once the ignitor is switched off. The details of the spark formation (momentum modification contribution, plasma and shock wave formation) are not considered in this DNS database for the purposes of simplicity and computational economy.

3. DNS database

The simulations have been carried out using the compressible three-dimensional DNS code `SENGA` [49] in a domain of size $55\delta_z \times 55\delta_z \times 55\delta_z$ or $6.5l_t \times 6.5l_t \times 6.5l_t$, where l_t is the integral length scale. This domain was not large enough to accommodate the development of the kernel for $t/t_{sp} \geqslant 5$ for moderate to high turbulence intensities (i.e. $u'/s_l^0 \geqslant 6$), and a larger domain of size $75\delta_z \times 75\delta_z \times 75\delta_z$ or $8.5l_t \times 8.5l_t \times 8.5l_t$ has been used. The small domain is discretised by a Cartesian grid of $512 \times 512 \times 512$ cells of uniform size Δx, while the larger domain is discretised with a grid of $700 \times 700 \times 700$ cells. This grid spacing ensures 10 grid points across the thermal flame thickness $\delta_{th} = [T_{\mathrm{ad}} - T_0] \,/\, \max(|\nabla \hat{T}|)$. It also ensures $\eta_k > \Delta x$, where η_k is the Kolmogorov length scale. The boundaries of the domain are considered to be partially non-reflecting and are specified using the Navier-Stokes Characteristic Boundary Conditions (NSCBC) technique [50]. The code employs a 10-th order central difference scheme for the internal points that gradually decreases to a one-sided 2^{nd}-order scheme at the non-periodic boundaries for the spatial differentiation. The time advancement is carried out using a 3^{rd}-order low-storage Runge-Kutta scheme [51].

The flammable mixture represents a stoichiometric methane/air mixture with $s = 4$, which with an oxygen mass fraction in pure air of $Y_{o,\infty} = 0.233$ yields the unburned gas fuel mass fraction as $Y_{f,st} = Y_{f,u} = 0.055$, whereas the burned fuel mass fraction is $Y_{f,b} = 0$. The mixture is preheated, such that $\tau = 3$, and the Zel'dovich number is $\beta = 6$ which is representative of methane/air combustion. Standard values have also been chosen for the Prandtl number ($\mathrm{Pr} = 0.7$), the ratio of specific heat ($\gamma = 1.4$) and the Lewis number is taken to be unity for all species.

The width and duration of the energy deposition are kept unaltered throughout the study and are similar to previous studies of localised forced ignition [26, 30–34] with $R_{sp}/\delta_z = 2.45$ and $b_{sp} = 0.2$ respectively. The ignitor centre is located at the geometric centre of the computational domain.

The flame-turbulence interaction takes place under decaying isotropic homogeneous turbulence. A well-known pseudo-spectral method [52] is used to initialise the turbulent velocity fluctuations with prescribed root-mean-square (rms) values (u') and integral length scale (l_t) obeying the Batchelor-Townsend spectrum

u'/s_l^0	l_t/δ_z	t_e/t_{sp}	Da	Ka	Case	Grid
0.00	9.0	–	–	–	I/P	S
0.50	9.0	90.0	18.0	0.12	I/P	S
1.00	9.0	45.0	9.00	0.33	I/P	S
1.50	9.0	30.0	6.00	0.61	I/P	S
2.50	9.0	18.0	3.60	1.32	I/P	S
4.00	9.0	11.2	2.25	2.67	I/P	S
6.00	9.0	7.5	1.50	4.90	I/P	I(S)/P(L)
9.00	9.0	5.0	1.00	9.00	I/P	I(S)/P(L)
11.5	9.0	3.9	0.78	13.0	I/P	I(S)/P(L)
14.0	9.0	3.2	0.64	17.5	I/P	I(S)/P(L)
18.0	9.0	2.5	0.50	25.5	I/P	I(S)/P(L)
22.0	9.0	2.0	0.41	34.4	I/P	I(S)/P(L)
27.0	9.0	1.7	0.33	46.8	I/P	I(S)/P(L)
32.0	9.0	1.4	0.28	60.3	I	S
37.0	9.0	1.2	0.24	75.0	I	S
41.0	9.0	1.1	0.22	87.5	I	S
45.0	9.0	1.0	0.20	101	I	S

Table 1: Initial turbulence properties and dimensionless parameters for the DNS database - I denotes the evaluation of the MIE for ignition only, I/P for ignition and propagation, while S indicates that the small computational domain (512^3) has been used while L indicates that the large one (700^3) has been used

[53]. The initial integral length scale is kept constant throughout the study at $l_t/\delta_z = 9$ (i.e. $l_t/\delta_{th} = 4.35$) and it remains comparable with previous computational studies of localised ignition [26, 30–34, 54, 55], but smaller than those used in experimental studies with $l_t/\delta_{th} \approx 6 - 7$ for Cardin *et al.* [11, 12] and $l_t/\delta_{th} \approx 40 - 90$ for Shy *et al.* [9] respectively. The different initial values of the normalised turbulent velocity u'/s_l^0 are listed in Tab. 1 alongside the ratio of initial eddy turnover time $t_e = l_t/u'$ and energy deposition duration t_{sp}. The Damköhler and Karlovitz number are also presented in Tab. 1 which shows that the combustion regimes investigated span from the wrinkled flamelet regime to the lower bound of the broken reaction zones regime. The cases with large values of u'/s_l^0 were deemed necessary in this work in order to evenly sample the wide range of turbulence intensities used, but also such that there would be enough data points to accurately evaluate the trends of the MIE variation with turbulence intensity for both $u'/s_l^0 \leqslant u'_c/s_l^0$ and $u'/s_l^0 \geqslant u'_c/s_l^0$ (where u'_c/s_l^0 denotes the critical turbulence intensity at which the MIE transition occurs). Note that for large values of the turbulence intensity (i.e $u'/s_l^0 \geqslant 32.0$), the MIE sufficient to obtain solely successful ignition has been evaluated because the developing flame kernels left the extended domain before it was possible to determine whether a self-sustained flame propagation was obtained or not.

The DNS simulations have been carried out for at least $t = 2t_{sp}$ for the evaluation of the MIE which is sufficient to ensure at least successful ignition. For each value of the turbulent parameters listed in Tab. 1, several simulations have been carried out with small variations of the ignition energy parameter a_{sp} to estimate the MIE to a precision of about 1% of the laminar MIE value. This represented roughly

100 computations, each of them lasting for up to 96h on 128 CPUs using Cirrus HPC[1]. By contrast, the simulations have been continued up to $t = 10t_{sp}$ to ensure that the burned gas mass continues to increase with time so as to evaluate the MIE which is sufficient for self-sustained growth of the kernel. The simulation time of $t \approx 10t_{sp}$ remains comparable to that used in previous analyses [26, 30–34, 54, 55]. For theses cases, the MIE was sought with an accuracy of about $3-5\%$ of the laminar MIE yielding a total number about 30 calculations on the $512 \times 512 \times 512$ grid, and 25 on the $700 \times 700 \times 700$ grid with computations lasting for up to 8 days on 250 CPUs. The overall analysis thus required more than 150 DNS simulations for a total computational cost of about 1.5 million CPUh.

4. Results

4.1. Flame-turbulence interaction

The non-dimensional temperature (T) iso-surfaces at different time instants are shown in Fig. 1 for different initial values of the turbulence intensity and $\Gamma = \Gamma^i_{\mathrm{MIE}}$ where the normalised energy Γ is defined as $\Gamma = \mathrm{IE}/\mathrm{MIE}^0_l$ where IE is the ignitor energy and MIE^0_l is the laminar MIE for self-sustained flame propagation and Γ^i_{MIE} is the normalised MIE to ensure at least successful ignition. In the present analysis, the laminar MIE is given by $\mathrm{MIE}^0_l / \left[\rho_0 C_p \tau T_0 \left(4/3\pi\delta_z^3\right)\right] = 4.7$. The difference in size of the $T = 0.1$ iso-surface at $t/t_{sp} = 0.5$ between initial $u'/s^0_l = 6$ and $u'/s^0_l = 27$ cases indicates that the energy requirement to obtain a successful ignition increases with increasing turbulence intensity. After the end of the energy deposition, $T = 0.3$ is reached at the centre of each of the developing kernels, and the temperature can be seen to increase in time until a small volume with $T \geqslant 1$ is obtained for all values of u'/s^0_l shown in Fig. 1. This increase is faster for higher u'/s^0_l as can be seen by the appearance of the $T = 1$ iso-surface at $t/t_{sp} \approx 1.5$ for the cases with initial $u'/s^0_l = 27$ and $u'/s^0_l = 18$ while it only appears at $t/t_{sp} \approx 2$ for the case with initial $u'/s^0_l = 6$. This indicates that the ignition is successful for each one of the cases presented here. Subsequently, the volume with $T \geqslant 1$ keeps increasing in time for the case with initial $u'/s^0_l = 6$ while it decreases for both initial $u'/s^0_l = 18$ and $u'/s^0_l = 27$ cases, indicating that the successful ignition may lead to a successful propagation in the first case, and a possible flame quenching in the second. Furthermore, the turbulence induced flame wrinkling can be seen from the increasing deviation from a spherical shape as u'/s^0_l increases and time progresses. For the initial $u'/s^0_l = 6$ case, the kernel shape remains roughly spherical, whilst as the turbulence intensity becomes larger, the kernel start to assume finger-like shapes, and may even be broken into multiple structures (see the case with initial $u'/s^0_l = 27$ at $t/t_{sp} = 2.5$ and 3) whilst the kernel is being quenched.

The non-dimensional temperature fields at the central mid-planes and the $T = 0.6$ iso-surfaces at different time instants are shown in Fig. 2 for cases with initial values of the turbulence intensity $u'/s^0_l = 0.0, 6.0, 18.0$

[1] http://www.cirrus.ac.uk/about/hardware.html

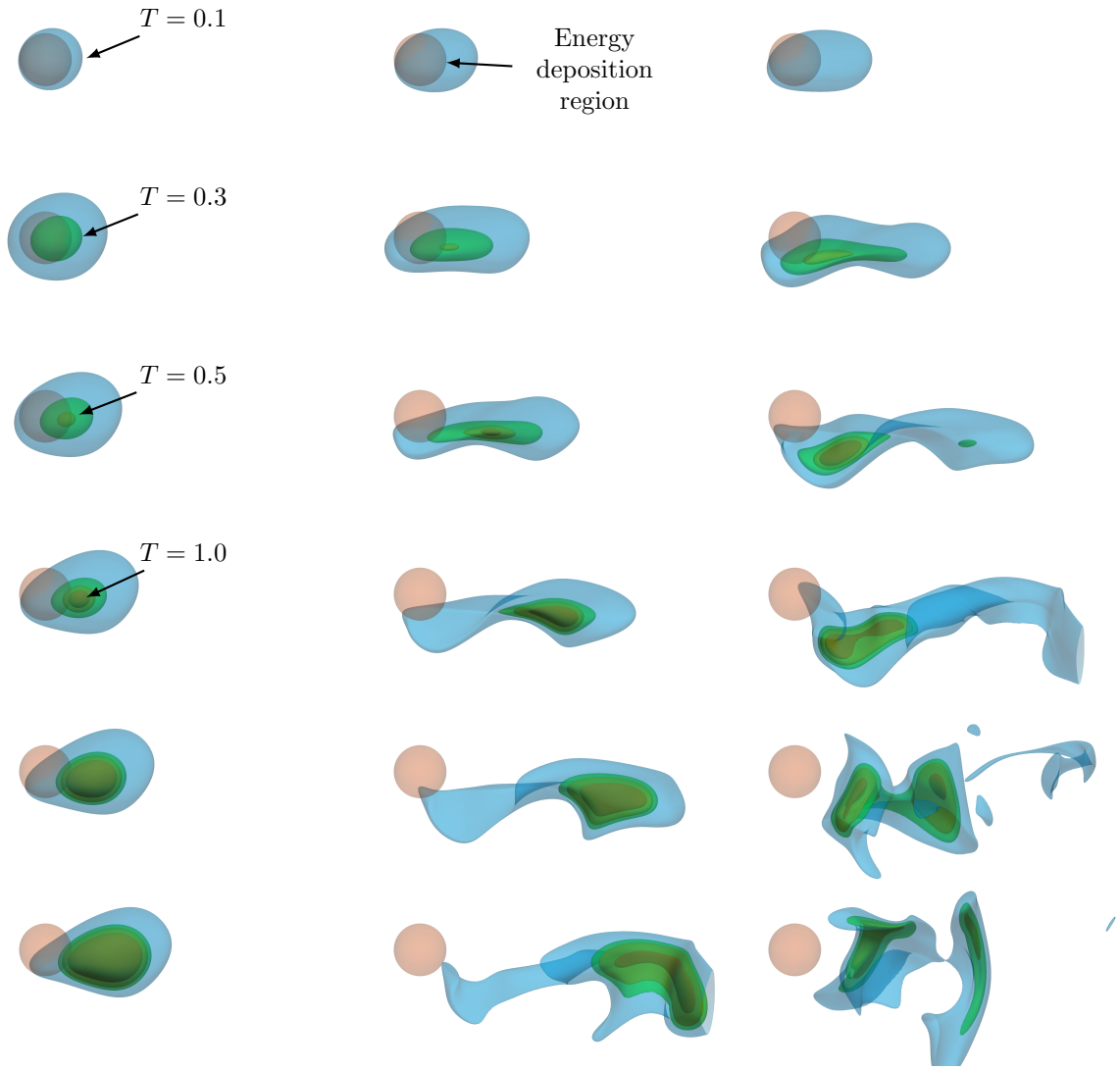

Figure 1: Isosurfaces of *(blue)* $T = 0.1$, *(green)* $T = 0.3$, *(orange)* $T = 0.5$ and *(red)* $T = 1$ with the energy deposition region indicated by the translucent red sphere obtained for $\Gamma = \Gamma^{i}_{\mathrm{MIE}}$ and *(left to right)* initial $u'/s_l^0 = 6,\ 18,\ 27$ at *(top to bottom)* $t/t_{sp} = 0.5,\ 1,\ 1.5,\ 2,\ 2.5,\ 3$

and $\Gamma = \Gamma^{p}_{\mathrm{MIE}}$ where $\Gamma^{p}_{\mathrm{MIE}}$ is the normalised MIE for self-sustained flame propagation. The iso-surface $T = 0.6$ is chosen as the fuel reaction rate magnitude assumes non-negligible values only for $T \geqslant 0.6$ for the present thermo-chemistry. From Fig. 2, it can be seen that the temperature isosurfaces remain perfectly spherical in the laminar case, and its volume increases as time progresses. At $t \leqslant t_{sp}$, for low to moderate initial values of u'/s_l^0, the kernels also retain a near spherical shape due to the diffusion of the energy deposited by the ignitor. For larger initial values of the turbulent velocity ($u'/s_l^0 \geqslant 14.0$), the turbulence significantly affects the kernel development and the flame loses its spherical shape. The $T = 0.6$ iso-surfaces expand with time, whilst they become increasingly wrinkled with increasing values of u'/s_l^0. Most notably, the flame kernels assume shapes which are increasingly far from spherical and exhibit finger-like features

generated by the turbulent vortical motion (e.g. $u'/s_l^0 = 18.0$). The centre of mass of the propagating kernels also moves away from the ignitor centre and may lie outside the flame kernels as the turbulence intensity increases.

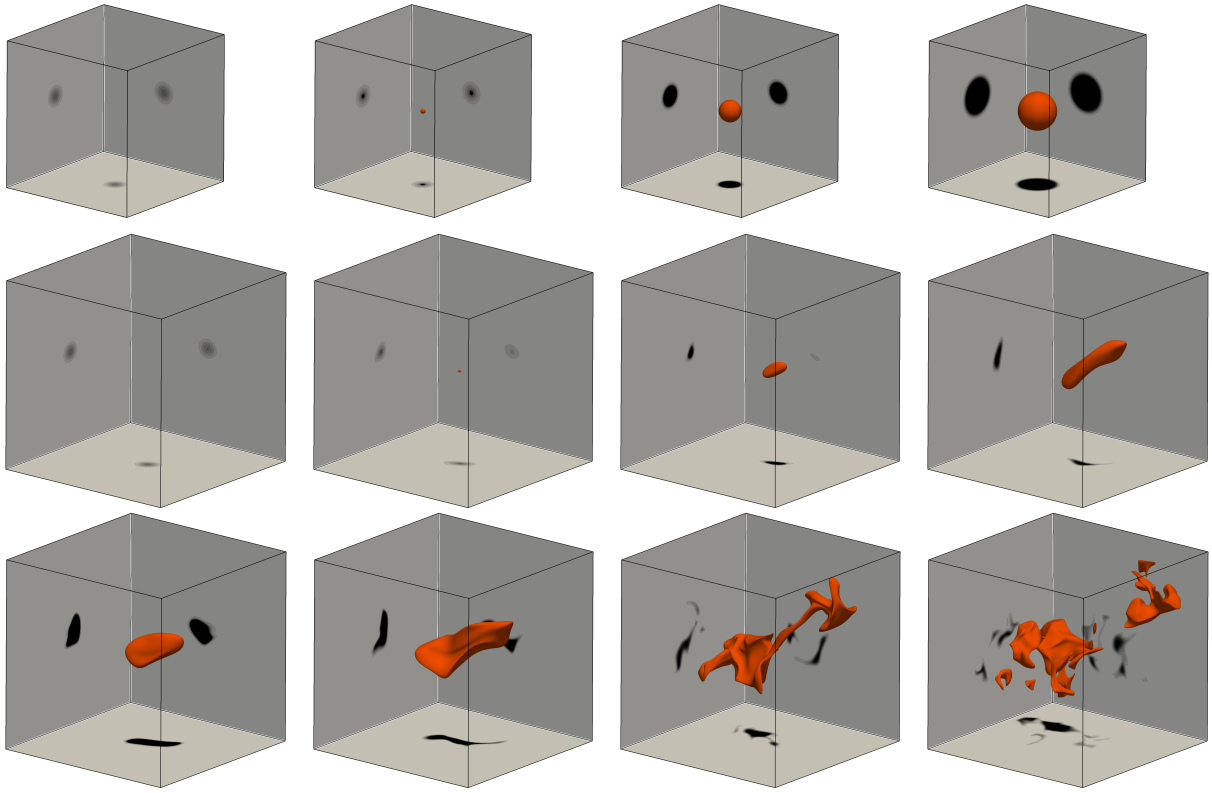

Figure 2: Isosurfaces of $T = 0.6$ for initial *(top to bottom)* $u'/s_l^0 = 0$, 6, 18 and at *(left to right)* $t/t_{sp} = 1$, 2, 4, 8 (5.2 on the bottom right) with the temperature field at the centre-planes (xy, xz and yz) projected on the sides of the domain in the case of $\Gamma = \Gamma^p_{\mathrm{MIE}}$ - Note that the computational domains are shown to scale

The extent of flame wrinkling can be quantified in terms of the magnitude of inner product of the local isotherm normal pointing towards the reactants $\mathbf{N} = -\nabla\hat{T}/|\nabla\hat{T}|$ and the radial unit vector $\mathbf{r}$ from the kernel centre of mass. For a perfectly spherical kernel (laminar case), the angle between $\mathbf{N}$ and $\mathbf{r}$ is zero (i.e. $|\cos(\theta)| = |\mathbf{N}\cdot\mathbf{r}| = 1.0$). The deviation of $|\mathbf{N}\cdot\mathbf{r}|$ from 1.0 thus provides a measure of flame wrinkling. The temporal evolution of $\Psi = \int_{V_{T\geqslant 0.6}} |\mathbf{N}\cdot\mathbf{r}|\,\mathrm{d}V/V_{T\geqslant 0.6}$ and $\Phi = d/R_{sp}$ (where d is the distance between the kernel mass and ignitor centres) are shown in Fig. 3 for $u'/s_l^0 = 0.0$, 4.0, 9.0, 18.0.

It can be seen from Fig. 3 that Ψ decreases, whereas Φ increases with increasing u'/s_l^0 and it becomes increasingly prominent as time progresses. For $u'/s_l^0 = 9.0$, and $t = t_{sp}$, the kernel mass centre appears to have moved to the edge of the energy deposition zone ($\Phi \approx 1.0$), while for larger values of u'/s_l^0, it leaves the energy deposition zone at $t/t_{sp} < 1.0$. This also suggests that it is not only the turbulent conditions at

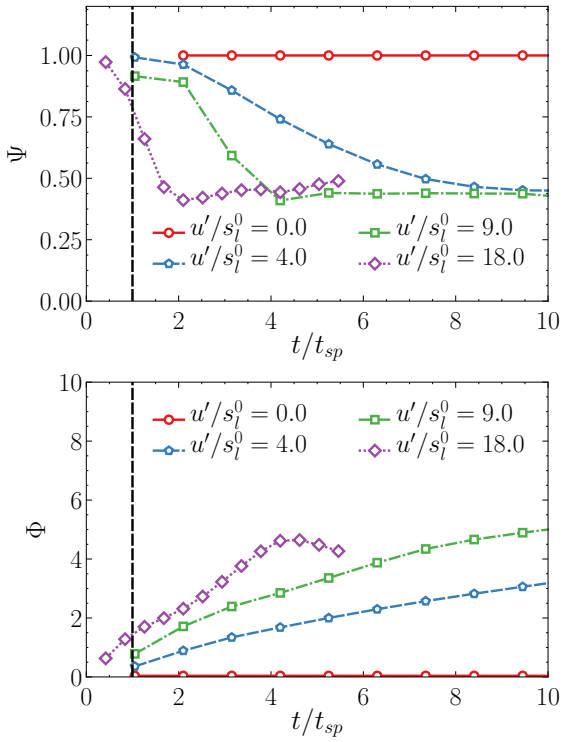

Figure 3: Temporal evolution of the *(top)* kernel wrinkling ($\Psi = \int_{V_T \geqslant 0.6} |\mathbf{N} \cdot \mathbf{r}| \, \mathrm{d}V / V_{T \geqslant 0.6}$) and *(bottom)* normalised distance between the kernel mass and ignitor centres ($\Phi = d/R_{sp}$) for initial turbulence intensities $u'/s_l^0 = 0.0$, 4.0, 9.0, 18.0 and $\Gamma = \Gamma^p_{\mathrm{MIE}}$

the ignitor location but also the flow conditions in the volume surrounding the ignitor that contribute to the possibility of ignition and subsequent flame propagation. Thus, the minimum energy that is required for self-sustained flame propagation is likely to be greater than the minimum energy requirement for just ignition, and this difference would increase with increasing u'/s_l^0. This can indeed be verified from Fig. 4 where the variations of normalised MIEs for both ignition (Γ^i_{MIE}) and self-sustained flame growth (Γ^p_{MIE}) are shown as a function of the turbulence intensity.

For low turbulence intensities, i.e $u'/s_l^0 \leqslant 6.0$, Γ_{MIE} is identical for both ignition and propagation. This is consistent with the findings of Fig. 3 indicating that the resulting flame kernel remains approximately spherical and its centre of mass does not move far from the ignitor. Hence, the local conditions under which a successful ignition is obtained are sufficient to give rise to a self-sustained flame propagation. At large values of u'/s_l^0, the energy needed to obtain a successful flame propagation becomes significantly larger than the one needed for successful ignition alone. It has already been observed from Fig. 3 that the hot gas kernel moves away from the ignitor and thus, the turbulent conditions under which a successful ignition is obtained may not be found at the location at which the kernel has moved. As a consequence, the kernel may not reach the critical radius (that increases with u'/s_l^0 [4]) for which self-sustained flame propagation

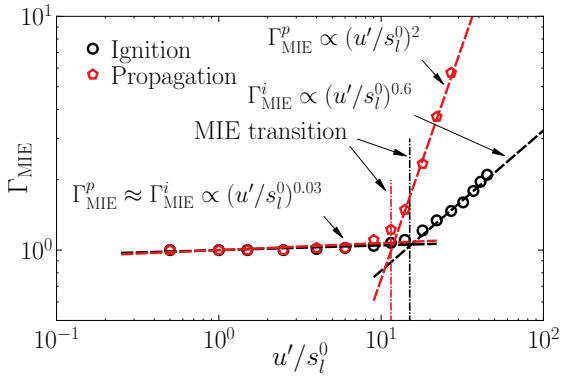

Figure 4: Normalised MIE for successful ignition ($\Gamma^i_{\rm MIE}$) and successful ignition followed by self-sustained flame propagation ($\Gamma^p_{\rm MIE}$) as a function of u'/s_l^0

is achieved. This, along with the uncertainty that the flame kernel will reach the critical radius during its motion away from the ignitor centre contributes to the greater values of $\Gamma^p_{\rm MIE}$ than $\Gamma^i_{\rm MIE}$ for large values of u'/s_l^0. Hence, successful ignition does not ensure self-sustained flame propagation, and the minimum energy required to ensure self-sustained flame propagation can be considerably greater than the minimum value which is sufficient to just ignite the mixture.

4.2. MIE transition

For both successful ignition and self-sustained flame propagation, two different regimes can be observed on Fig. 4, with a slow increase of $\Gamma^i_{\rm MIE}$ and $\Gamma^p_{\rm MIE}$ with turbulence intensity for low values of u'/s_l^0 and a large increase as the turbulence intensity increases. The critical turbulence intensity at which a transition is observed for ignition is approximately $u_c'^i/s_l^0 \approx 14.0$ and it decreases slightly to $u_c'^p/s_l^0 \approx 11.5$ for self-sustained propagation. This is slightly smaller than the experimental results of Shy *et al.* [9] which reported $u_c'^p/s_l^0 \approx 15.0$ for a stoichiometric methane/air mixture, and larger than the value of $u_c'^p/s_l^0 \approx 7.0 - 10.0$ reported by Cardin *et al.* [11, 12] for lean methane/air mixtures with $0.55 \leqslant \phi \leqslant 0.75$. The critical Karlovitz number ($\mathrm{Ka}_c = \left(u_c'/s_l^0\right)^{3/2} \left(l_t/\delta_z\right)^{-1/2}$) is thus approximately 17.0 (i.e. $\mathrm{Ka}_c^i \approx 17.0$) for ignition and $\mathrm{Ka}_c^p \approx 13.0$ for successful self-sustained flame propagation, while Shy *et al.* [9] experimentally obtained $\mathrm{Ka}_c^p \approx 8.0$ and Cardin *et al.* [11, 12] observed $\mathrm{Ka}_c^p \approx 10.0$ for fuel-lean mixtures.

Based on the current DNS data, the propagation MIE dependence on the turbulent intensity in the two regimes can be approximated as $\Gamma^p_{\rm MIE} \propto \left(u'/s_l^0\right)^n$ with $n = 0.03$ for $u'/s_l^0 \leqslant u_c'^p/s_l^0$ and $n = 2$ for $u'/s_l^0 \geqslant u_c'^p/s_l^0$.

It was experimentally found by Shy *et al.* [9] that n varies between 1.0 for $u'/s_l^0 \leqslant \left(u'/s_l^0\right)_c$ to $n = 7 - 16$ for $u'/s_l^0 \geqslant \left(u'/s_l^0\right)_c$ for methane/air mixtures at different equivalence ratios. The quantitative disagreement between the experimental data reported by Shy *et al.* [9] and the DNS data can be attributed to differences in the measurement of the energy deposited. In electric spark ignition, the energy transferred from the

electrodes to the fluid is not precisely known and varies significantly based on the electrodes material, size, geometry and gap width but also depends on the duration, profile and total energy of the discharge, to which additional heat losses due to the forced convection must be accounted for. From the energy transferred to the fluid, some is further lost due to plasma formation and the creation of an initial shock wave. Thus, the amount of energy that is finally used for an increase of the fluid temperature is much lower and non-linearly related to the total energy measured at the electrodes. This differs from the DNS in which all the energy added to the flow is fully converted into a temperature increase. As already pointed out, the integral length scales also differ significantly between the experiment and the simulations, with $l_t/\delta_{th} = 4.35$ in the current DNS analysis and $l_t/\delta_{th} \approx 40 - 90$ in the experiment [9].

Undeniably, the background turbulence has a large impact on the MIE and its variation as a function of the turbulence intensity. It will be discussed and demonstrated later that the success of ignition and subsequent flame propagation without the aid of an external energy source depends on the competition between the chemical heat release rate and the heat transfer rate from the hot gas kernel. Heat transfer has an adverse effect on the likelihood of both ignition and subsequent self-sustained combustion, as it scales with the rms velocity fluctuation u'. Thus, if forced turbulence were to be used, u' would not decay and the heat transfer from the hot gas kernel would increase in comparison to the heat transfer under decaying turbulence. This in turn would mean that the MIE would increase from the values found for decaying turbulence, as the higher heat transfer from the hot gas kernel would result in a misfire or flame quenching if the MIE found for decaying turbulence was to be used for forced turbulence. The results would not change qualitatively as the competition between the heat release rate and heat transfer will still determine the magnitude of the MIE, but quantitatively, some differences are expected. The laminar MIE energy will not depend on whether the turbulence is decaying or maintained. Consequently, if forced turbulence were to be used instead of decaying turbulence, two key changes in the results would be observed : *(1)* the MIE for each turbulence intensity other than $u'/s_l^0 = 0$ would increase, and the level that it would change by compared to the decaying turbulence is expected to increase with increasing u'/s_l^0, and *(ii)* due to the increase of the MIE values (but the identical value of MIE at $u'/s_l^0 = 0$), it is expected that the evolution of Γ_{MIE} across the values of u'/s_l^0 both smaller and larger than u'_c/s_l^0 would become steeper.

When comparing the current results with data from a different experimental set-up which uses a much smaller integral length scale ($l_t/\delta_{th} \approx 6 - 7$), decaying turbulence and laser ignition (which deposits energy in a more precise manner than sparks) [11, 12], the quantitative agreement improves significantly. It was indeed reported by Cardin *et al.* [11, 12] that $n = 0.01 - 0.1$ for $u'/s_l^0 \leqslant u_c'^p/s_l^0$ and $n = 1.4 - 2.1$ for $u'/s_l^0 \geqslant u_c'^p/s_l^0$. However, the present analysis is done for a stoichiometric methane-air mixture whereas the analysis presented by Cardin *et al* [11, 12] considered fuel-lean mixtures. It is important to note that the slopes for the normalised MIE variation with u'/s_l^0 for the experimental data by Cardin *et al* [11, 12] do not change significantly with the variation of equivalence ratio for $u'/s_l^0 \geqslant (u'/s_l^0)_c$. For the present

thermo-chemistry, the physical processes which determine the MIE do not change appreciably with the equivalence ratio apart from the decreasing magnitude of the fuel reaction rate with increasing departure from the stoichiometric mixture. This would lead to an increase of the MIE value with decreasing equivalence ratio for fuel-lean mixtures [4–7, 26] but a limited number of simulations indicated that the normalised MIE (i.e. Γ_{MIE}) does not change noticeably with the equivalence ratio. Thus, the variation of Γ_{MIE} with u'/s_l^0 in Fig. 4 is not likely to change significantly with different equivalence ratios.

Finally, a notable difference exists in the methodology used to measure the MIE in the experimental and numerical analysis. It can be first remarked that the MIE measured experimentally is defined statistically at 50% ignitability due to the existence of a region of ignition energy within which successful flame propagation and flame quenching co-exist even under the same statistical turbulent background. This is due to the fact that experimentally, the turbulent background are statistically identical but locally different, and that the amount of energy deposited in the mixture is only approximately known. Based on the work of Shy and co-workers [8, 9] and particularly on the presentation of the MIE determination [9, Appendix A] and the work of Cardin *et al.* [11, 12], it can be inferred that more that 3000 experimental runs were needed in the first case and more than 800 in the second. Experimentally, different statistical turbulent flow fields were generated and energy was deposited incrementally, such that both 0% and 100% ignitability thresholds can be determined. Further energy deposition events allow the determination of the 50% ignitability value using a spline fitting method. To follow the same methodology numerically would be exorbitantly expensive and outside the means of most research groups using the DNS tool. Thus, the current work does not capture the MIE at 50% ignitability as understood experimentally, but rather determines the MIE as a threshold value. Here, the MIE is reported based on a realisation which showed successful ignition/self-sustained propagation, and the number of successful events was then measured by depositing identical amounts of energy to different realisations with statistically similar turbulence properties as detailed below.

4.3. Temporal evolution

The temporal evolutions of the maximum value of non-dimensional temperature (T_{max}), maximum normalised fuel reaction rate magnitude ($\dot{\omega}_f^* = |\dot{\omega}_{f,\mathrm{max}}| \times \delta_z/\rho_0 s_l^0$) and the volume defined by $c \geqslant 0.5$ normalised by the ignitor volume $V_{sp} = 4/3\pi R_{sp}^3$ are shown in Fig. 5 for different turbulence intensities and normalised energies close to Γ_{MIE}^i.

The behaviour observed here matches previous numerical results [21, 26, 30], with the maximum temperature increasing continuously during the energy deposition up to $T_{\mathrm{max}} \approx 0.5$ for all values of u'/s_l^0. At $t/t_{sp} = 1$, chemical reactions remain small (see the low values of $\dot{\omega}_f^*$) and the large thermal gradient created by the energy deposition gives rise to a high energy transfer that heats the surrounding unburned mixture. Later on, at $t/t_{sp} \geqslant 1.1$, if the heat release is strong enough, T_{max} keeps increasing until a thermal runaway occurs when the temperature reaches a value close to $T_c = 1 - 1/\beta$. Under these conditions, the

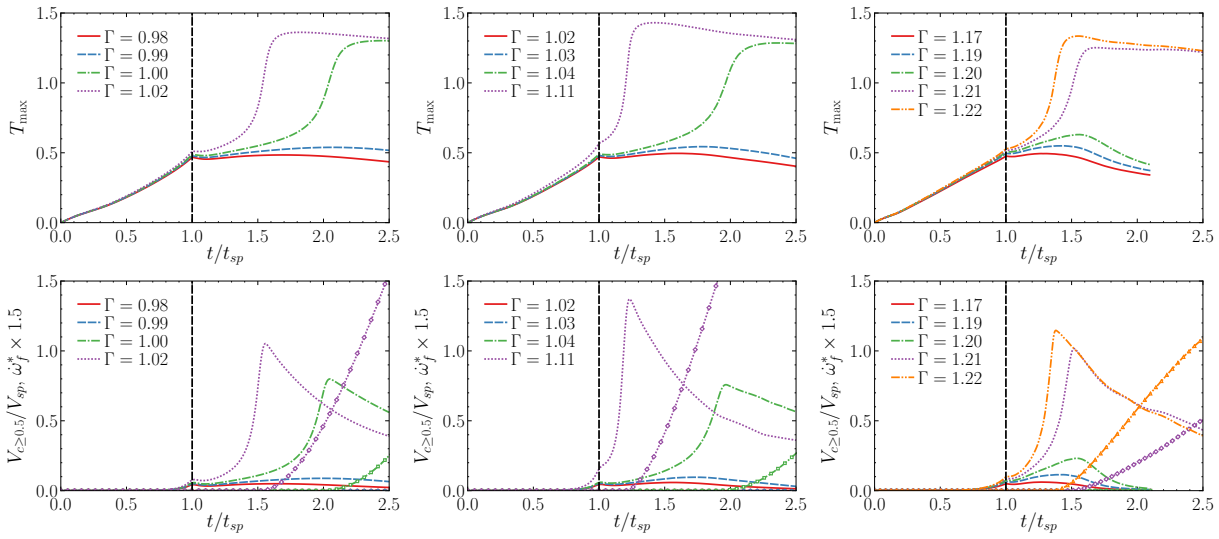

(a) $u'/s_l^0 = 0.0$ **(b)** $u'/s_l^0 = 9.0$ **(c)** $u'/s_l^0 = 18.0$

Figure 5: Temporal evolution of *(top row)* $T_{\max}$ and *(bottom row)* (symbols) $V_{c\geqslant 0.5}/V_{sp}$ and (lines) $\dot{\omega}_f^* = |\dot{\omega}_{f,\max}| \times \delta_z/\rho_0 s_l^0$ at different initial values of u'/s_l^0 and ignition energies close to Γ^i_{MIE} - The vertical black dashed line indicates $t/t_{sp} = 1$

non-dimensional temperature T then reaches a maximum larger than unity (i.e. $T_{\max} > 1$) and the ignition is successful. Simultaneously, the maximum value of the reaction rate magnitude increases rapidly to reach a maximum. It subsequently decreases as the fuel availability diminishes, and only then, the maximum temperature starts to decrease. It can also be remarked that in ignition events, the reaction progress variable and the temperature are decoupled in the early stages. The maximum temperature has already reached values greater than unity, while the volume of burned gas $V_{c\geqslant 0.5}$ is still zero. This decoupling then decreases as the maximum temperature decreases to reach $T_{\max} = 1$, at which point, both the progress variable and the temperature becomes coupled.

It is worth mentioning that all ignition events visible in Fig. 5 can be considered as autoignition events as the thermal runaway occurred long after the energy deposition has ended. In fact, at $t = t_{sp}$, the volume of products is still zero and only starts to increases after the thermal runaway. The joint probability density functions (jPDFs) of the normalised heat release and normalised temperature dissipation rate defined by $\chi_T = \lambda/(\rho_0 C_p)\nabla T \cdot \nabla T$ are presented in Fig. 6 at different time instants for $u'/s_l^0 = 9.0$, $\Gamma = \Gamma^i_{\text{MIE}}$ and $T = 0.3$. A clear negative correlation between $\dot{\omega}_T$ and χ_T can be observed at $t = 0.78t_{sp}$ with $\underline{p} = -0.92$ (where $\underline{p} = \text{Cov}(\dot{\omega}_T,\ \chi_T)/\sigma_{\dot{\omega}_T}\sigma_{\chi_T}$ is the correlation coefficient, $\text{Cov}(\lambda_i,\ \lambda_j)$ indicates the co-variance of scalars λ_i and λ_j and σ_{λ_i} the variance of scalar λ_i), which is indicative of an autoignition event [42, 56]. The value of $\underline{p}$ then increases with time, and at $t/t_{sp} = 1.05$ it is positive with $\underline{p} = 0.25$, until it stabilises at $\underline{p} \approx 0.6$ at $t/t_{sp} \approx 2.5$, which is representative of a premixed flame. It has also been found that the magnitude of $\dot{\omega}_T$ remains much greater than that of $\nabla \cdot (\lambda \nabla \hat{T})$ when the temperature runaway takes place for the cases with initially $u'/s_l^0 \leqslant 11.5$ (not shown here), which is also indicative of an autoignition event.

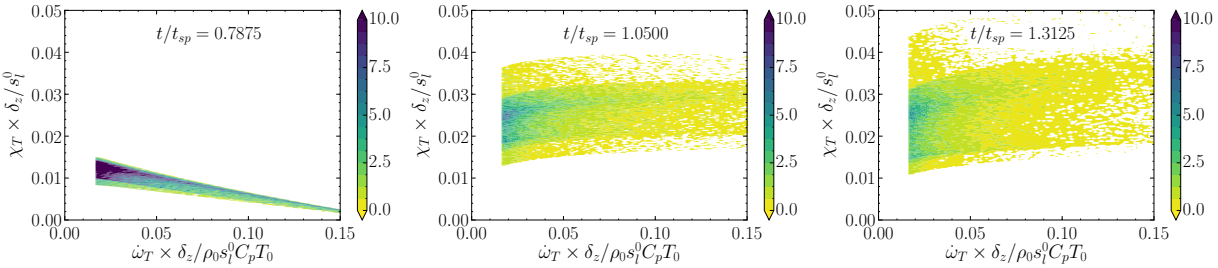

Figure 6: jPDFs of normalised heat release ($\dot{\omega}_T \times \delta_z/\rho_0 s_l^0 C_p T_0$) and normalised temperature dissipation rate ($\chi_T \times \delta_z/s_l^0$) for $u'/s_l^0 = 9.0$ and $\Gamma = \Gamma^i_{\mathrm{MIE}}$ on the $T = 0.3$ iso-surface

Figure 7 presents the evolution of the maximum temperature, normalised maximum fuel reaction rate magnitude and burned gas volume at different turbulent intensities and $\Gamma = \Gamma^p_{\mathrm{MIE}}$. For low turbulence intensities (i.e. $u'/s_l^0 \leqslant 1.5$), the turbulence does not have any effect on the occurrence of the self-sustained flame propagation, which can be seen through the similarity of the different temporal evolutions for different turbulent intensities. This is also consistent with the finding that the MIE is almost independent of the turbulence intensity at low values of u'/s_l^0 reported by Cardin *et al.* [11, 12]. For moderate turbulence intensities (i.e. $2.5 \leqslant u'/s_l^0 \leqslant 9.0$), the energy demand for ensuring self-sustained flame propagation increases, as shown by the thermal runaways occurring earlier but still after the end of the energy deposition, indicating that these events are still auto-ignition events. The peak reaction rate magnitude also increases with u'/s_l^0 (by almost 50% from $u'/s_l^0 = 2.5$ to $u'/s_l^0 = 9.0$). The auto-ignition events can be found up to $u'/s_l^0 \approx 11.5$ but disappear for larger values of the initial turbulence intensity. Indeed, as u'/s_l^0 increases, Γ^p_{MIE} also increases leading to the maximum temperature reaching unity at $t/t_{sp} \leqslant 1$ before it reaches a maximum at $t/t_{sp} = 1$. Consequently, the peak reaction rate is found before the end of the energy deposition, before a rapid decrease is observed as the reactants are fully converted to products within the ignitor volume. A short stabilisation can then be observed, when the fuel concentration reaches zero while energy is still deposited by the ignitor leading to a large diffusion of temperature through the flame front. At $t/t_{sp} = 1$, the reaction rate decreases sharply, and the burned gas volume is already very large with $V_{c\geqslant 0.5}/V_{sp} \geqslant 10.0$ for $u'/s_l^0 = 18.0$. At later times, the temperature decreases slowly until it eventually reaches unity as the hot gas volume increases, indicating that self-sustained combustion is occurring.

4.4. Stochastic behaviour

The success of ignition is extremely sensitive to the amount of energy deposited, as shown in Fig. 5 where an increase by 1% of Γ is enough to obtain a thermal runaway and a successful ignition. To investigate the influence of turbulence on this fundamentally stochastic process, two additional simulations have been run with $\Gamma = \Gamma^i_{\mathrm{MIE}}$ and $\Gamma = \Gamma^p_{\mathrm{MIE}}$ for each value of u'/s_l^0 presented in Tab. 1. Each one of these two additional simulations has been run with a statistically identical (i.e. u'/s_l^0 and l_t) but locally different realisation of the initial turbulent field. The outcome of the energy deposition in locally different, but statistically identical,

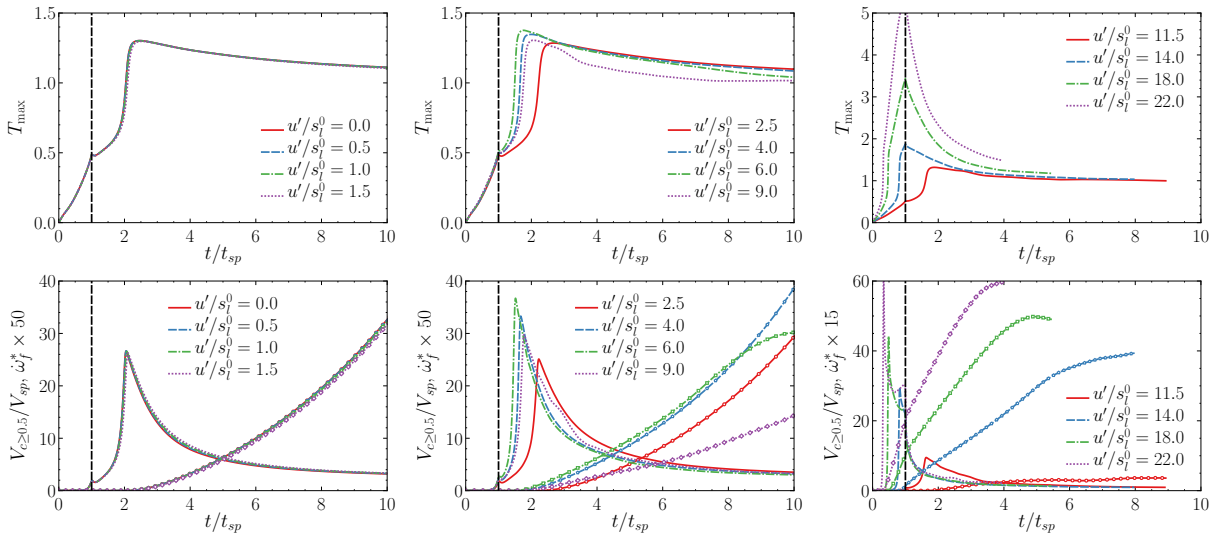

(a) $0.0 \leqslant u'/s_l^0 \leqslant 1.5$ **(b)** $2.5 \leqslant u'/s_l^0 \leqslant 9.0$ **(c)** $11.5 \leqslant u'/s_l^0 \leqslant 22.0$

Figure 7: Temporal evolution of *(top row)* $T_{\max}$ and *(bottom row)* (symbols) $V_{c\geqslant 0.5}/V_{sp}$ and (lines) $\dot{\omega}_f^* = |\dot{\omega}_{f,\max}| \times \delta_z/\rho_0 s_l^0$ for different initial values of u'/s_l^0 and $\Gamma = \Gamma^p_{\text{MIE}}$ during self-sustained flame propagation - The vertical black dashed line indicates $t/t_{sp} = 1$

initial turbulent flow fields with $\Gamma = \Gamma^i_{\text{MIE}}$ and $\Gamma = \Gamma^p_{\text{MIE}}$ is reported in Fig. 8 for different initial turbulence intensities.

It is worth noting that Fig. 8 indicates whether the minimum energy necessary to obtain a successful ignition/propagation for one particular turbulent realisation also corresponds to the minimum energy necessary to obtain a successful ignition/propagation for other statistically similar realisations. Subsequently, there is always at least one successful event for each turbulence intensity, associated with the realisation, which is referred to as realisation 1.

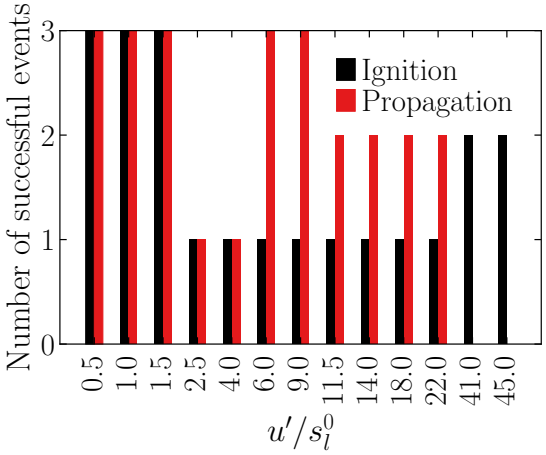

Figure 8: Number of successful events out of three different turbulent realisations at different initial values of u'/s_l^0 with $\Gamma = \Gamma^i_{\text{MIE}}$ (ignition) or $\Gamma = \Gamma^p_{\text{MIE}}$ (propagation) - Note that self-sustained propagation has not been investigated for $u'/s_l^0 \geqslant 27.0$

It can be seen that for low values of u'/s_l^0 (i.e. $u'/s_l^0 \leqslant 1.5$), different realisations of turbulence do not influence the number of successful events. However, as u'/s_l^0 increases, failed ignition is obtained for some realisations of statistically identical turbulent flow fields, and this behaviour persists until the very large turbulence intensities (i.e. $u'/s_l^0 > 37.0$). For $u'/s_l^0 \geqslant 41.0$, the eddy turnover time becomes comparable to the energy deposition time, i.e. $t_e/t_{sp} \approx 1.0$ (see Tab. 1), and this allows some fluid to receive energy multiple times due to the turbulent motion that brings it back within the ignitor volume before the end of the energy deposition. The probability of successful propagation is not 100% for $u'/s_l^0 = 2.5$ and 4.0 where $\Gamma = \Gamma^i_{\mathrm{MIE}} = \Gamma^p_{\mathrm{MIE}}$, which means that the failed propagations here are misfires. Consequently, up to moderate turbulent intensities (i.e. up to $u'/s_l^0 \approx 9.0$), if the ignition is successful, the combustion will become self-sustained. For larger values of u'/s_l^0 (i.e. $u'/s_l^0 \geqslant 11.5$), the probability of self-sustained propagation decreases to about 66.6% as turbulence starts to affect the later stages of the kernel development.

Figure 9 shows the temporal evolution of $T_{\max}$ for the different turbulent realisations at several values of initial u'/s_l^0 and $\Gamma = \Gamma^i_{\mathrm{MIE}}$. For $u'/s_l^0 = 1.0$, the temperature profiles appear similar with an almost identical temperature at $t = t_{sp}$, but a slight time lag (i.e. $\Delta t \approx 0.1 t_{sp}$) in reaching the adiabatic flame temperature can be observed. Three successful ignitions for all three different turbulent realisations are visible, and this is reported in Fig. 8 for $\Gamma = \Gamma^i_{\mathrm{MIE}}$. For larger turbulence intensities, the ratio t_e/t_{sp} decreases, and turbulent motions become more pronounced during the energy deposition. By increasing the local heat transfer rate, they are able to significantly decrease the maximum temperature reached leading to a misfire (Figs. 9b and 9c). For $u'/s_l^0 = 9$, a successful ignition is obtained for realisation 1, but misfires are obtained for both realisations 2 and 3, and this is represented in Fig. 8 where for $\Gamma = \Gamma^i_{\mathrm{MIE}}$ a single successful event is reported. The same method has been applied for each turbulence intensity shown in Fig. 8. This aims at giving an estimation of the ignitability percentage obtained for Γ^i_{MIE} and Γ^p_{MIE} respectively.

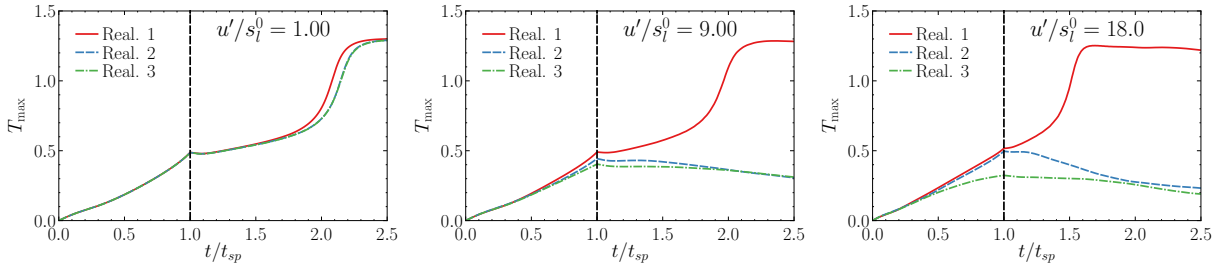

Figure 9: Temporal evolution of $T_{\max}$ for three turbulent realisations with $\Gamma = \Gamma^i_{\mathrm{MIE}}$ and different initial values of u'/s_l^0 - The vertical black dashed line indicates $t/t_{sp} = 1$

Figure 10 shows the temporal evolution of $V_{c\geqslant 0.5}/V_{sp}$ for similar turbulent conditions and $\Gamma = \Gamma^p_{\mathrm{MIE}}$. The choice of showing $V_{c\geqslant 0.5}/V_{sp}$ is substantiated by the fact that $T_{\max}$ remains greater than unity for a long time after ignition when using $\Gamma = \Gamma^p_{\mathrm{MIE}}$, and thus, does not constitute a good marker of the self-sustained growth of the kernel. For $u'/s_l^0 = 1.0$, the kernel volumes are very similar between the different realisations,

and the same slight lag observed for the ignition is also observed, which is due to $\Gamma = \Gamma^i_{\mathrm{MIE}} = \Gamma^p_{\mathrm{MIE}}$. For larger values of u'/s_l^0, the product volumes $V_{c\geqslant 0.5}/V_{sp}$ start to behave differently depending on the turbulent flow field (Figs. 10b and 10c). At $u'/s_l^0 = 9.0$, for example, realisation 1 has a volume which represents only 50% of the volume obtained with realisation 3 at $t/t_{sp} = 10$. This stems from a delay in the start of burning, indicating that the heat in realisation 3 might have been deposited within a larger volume of fluid due to the local turbulent motions. On Fig. 10c, the profiles are shown up to the time at which the kernel leaves the computational domain which happens at roughly $t/t_{sp} \approx 5$ for all realisations, at which point, the hot gas volume of realisation 2 has started to decrease indicating a possible failed propagation event.

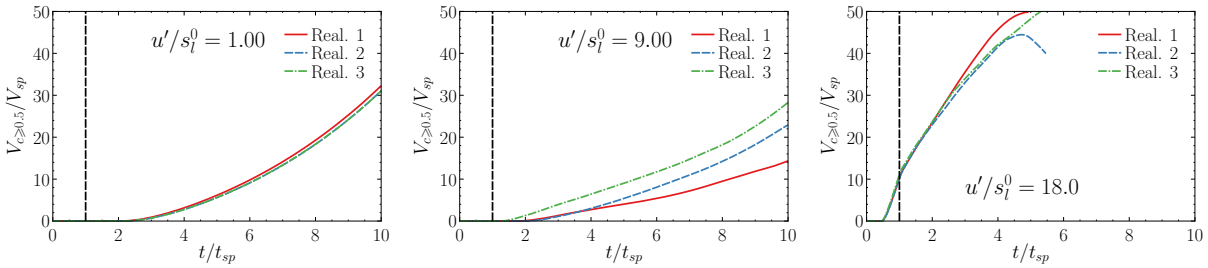

Figure 10: Temporal evolution of $V_{c\geqslant 0.5}/V_{sp}$ for three turbulent realisations with $\Gamma = \Gamma^p_{\mathrm{MIE}}$ and different initial values of u'/s_l^0 - The vertical black dashed line indicates $t/t_{sp} = 1$

4.5. Energy budget

An accurate understanding of the underlying mechanisms governing the ignition can be gained by analysing the energy balance. The temporal evolution of the energy equation budget (Eq. 3) is presented in Fig. 11 for $u'/s_l^0 = 9.0$, $\Gamma = \Gamma^i_{\mathrm{MIE}}$ and for the three turbulent realisations. Note that qualitatively similar results are obtained for the other values of u'/s_l^0 studied in this work.

For $t/t_{sp} \leqslant 1$, the mean contribution of the ignition source term P_3 is non-zero and at its maximum for high values of T found at the ignitor centre (see Fig. 2). The viscous term (D_1, not shown here for clarity) is not a leading order contributor and does not play any significant role in the ignition dynamic. The mean value of the convective (C_1) and pressure work (P_1) terms are linked through dilatation and follow similar trends. At early times, they are both negative as the reactants are pushed outwards, then at $t/t_{sp} \approx 1.3$, the sign changes and they both become positive for a short period of time. This is explained by the pressure equilibrating to the conditions found within the kernel, due to the absence of energy addition and the chemical heat release not being strong enough to sustain the kernel growth. At a later time, if the ignition is successful, C_1 and P_1 become negative again. The mean values of thermal diffusion D_2 and heat release P_2 are the leading order contributors in established flames [25] and a net positive mean value of $(P_2 + D_2)$ for a given T-isosurface indicates that it propagates into the unburned gas mixture. By contrast, the kernel shrinks if the positive heat release rate term P_2 is overcome by the negative contribution of the diffusion term D_2 (i.e. $P_2 + D_2 < 0$). At $t/t_{sp} \approx 0.75$, the mean value of P_2 is negligible, while the mean

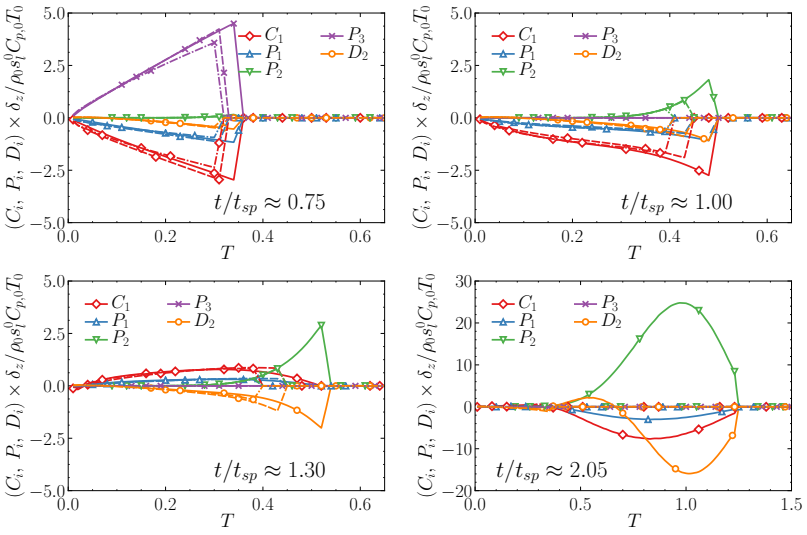

Figure 11: Energy budget for $u'/s_l^0 = 9.0$, $\Gamma = \Gamma^i_{\mathrm{MIE}}$ at different time instants and for different turbulent realisations (—— Real. 1, - - - Real. 2, -·-·- Real. 3)

value of D_2 is negative due to the large temperature gradients found at the ignitor centre. The magnitudes of both P_2 and D_2 increase with time and they eventually become leading order contributors to the energy transport shortly after the energy deposition ends (i.e. $t/t_{sp} \approx 1.3$). After the thermal runaway occurring at $t/t_{sp} \approx 1.9$ the mean values of both P_2 and D_2 for realisation 1 increase by an order of magnitude, before decreasing slowly as $T_{\max}$ decreases. For realisations 2 and 3, the mean values of both P_2 and D_2 decrease after the ignitor has been switched off due to failed ignition, which can be seen from the negative mean value of $(P_2 + D_2)$.

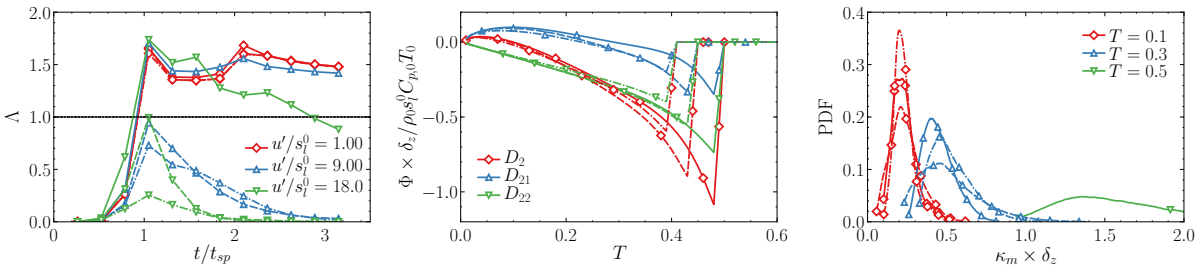

Figure 12: *(a)* Temporal evolution of $\Lambda = \max(|\langle P_2|_T\rangle|)/\max(|\langle D_2|_T\rangle|)$ for different values of u'/s_l^0 with $\Gamma = \Gamma^i_{\mathrm{MIE}}$, *(b)* Decomposition of the thermal diffusion rate term D_2 into its normal (D_{21}) and tangential (D_{22}) components for $u'/s_l^0 = 9.0$, $\Gamma = \Gamma^i_{\mathrm{MIE}}$ and $t/t_{sp} \approx 1.00$ and *(c)* PDF of κ_m on different isotherms for $u'/s_l^0 = 9.0$, $\Gamma = \Gamma^i_{\mathrm{MIE}}$ and $t/t_{sp} \approx 1.00$ - All the results are presented for different turbulent realisations (—— Real. 1, - - - Real. 2, -·-·- Real. 3)

Figure 12a presents the temporal evolution of the competition between the chemical heat release and thermal diffusion through the ratio $\Lambda = \max(|\langle P_2|_T\rangle|)/\max(|\langle D_2|_T\rangle|)$, where $\langle \ldots|_T\rangle$ denotes the conditional mean on temperature evaluated over the whole domain. If $\Lambda > 1$, the hot gas kernel expands in size, if

$\Lambda < 1$, the flame quenches. It can be observed that a marker of successful ignition is $\Lambda > 1$ at $t/t_{sp} = 1.0$, which would indicate that the occurrence of a thermal runaway is fully determined at $t/t_{sp} = 1.0$. However, the value of $T_{\max}$ reached at $t/t_{sp} = 1.0$ is not the only parameter governing Λ. This is highlighted by the very different values of Λ reached at $t/t_{sp} = 1.0$ across the different realisations although relatively similar $T_{\max}$ values are observed on Fig. 9.

Thus, the statistical behaviour of D_2 plays a key role in determining the success or failure of an ignition event. To study this effect, D_2 can be decomposed ($D_2 = D_{21} + D_{22}$) into its normal $D_{21} = \mathbf{N} \cdot \nabla(\lambda \mathbf{N} \cdot \nabla \hat{T})$ and tangential components $D_{22} = -\lambda |\nabla \hat{T}| \nabla \cdot \mathbf{N} = -2\lambda \kappa_m |\nabla \hat{T}|$, where $\kappa_m = 1/2 \nabla \cdot \mathbf{N}$ is the local curvature of isotherms. The curvature assumes a positive (negative) value for the surface elements which are convex (concave) to the unburned gas. This decomposition is shown for $u'/s_l^0 = 9$, $\Gamma = \Gamma^i_{\mathrm{MIE}}$ and for all turbulent realisations in Fig.12b at $t/t_{sp} \approx 1.0$. The mean value of the tangential diffusion contribution (D_{22}) (which is proportional to the isotherms curvature) conditional upon T, behaves similarly for all realisations. This is consistent with the fact that at such early times, the mean isotherm curvature is mainly driven by the thermal diffusion from the ignitor centre where the energy is deposited within the characteristic distance R_{sp}. However, the mean behaviour of the normal diffusion component (D_{21}) differs significantly depending on the realisations.

In order to understand this behaviour it is worthwhile to examine the PDF of κ_m, shown in Fig. 12c for different isotherms and realisations. The curvature distribution is wider for realisations 2 and 3 than for the first one on isotherm $T = 0.3$, indicating that κ_m can have large magnitudes locally and that significant local variations of D_{22} exist, although its mean value remains mostly unaffected. However, local behaviours of $|\nabla T|$ and D_{21} are also affected by the local value of κ_m.

To further investigate these local behaviours, the jPDFs of κ_m with $|\nabla T|$ and D_{21} for the three turbulent realisations are shown on Fig. 13. A clear negative correlation exists between the mean curvature and $|\nabla T|$, with $\underline{p} \approx -0.8$ for all turbulent realisations, which is consistent with earlier findings by Klein *et al.* [57]. A negative correlation also exists with the normal diffusion rate (D_{21}) which can be explained by the fact that as the mean curvature locally increases, the temperature gradient magnitude decreases and thus $-|\nabla T|$ increases with curvature. Furthermore, as shown in Fig. 6 at $t/t_{sp} = 1.05$, when the temperature gradient decreases, the reaction rate decreases as well, which brings down the temperature difference across the turbulent flamelet, and accordingly increases the distance between two given isotherms (Δx_f). The relative strengths of these mechanisms give rise to a negative correlation between D_{21} (which scales as $D_{21} \sim -\lambda \Delta T / \Delta x_f$) and κ_m. As the curvature locally takes larger values for realisations 2 and 3, the variation of the normal diffusion term also increases. Consequently, the magnitude of the diffusion rate may locally assume highly negative values that supersede the heat release rate leading to a misfire.

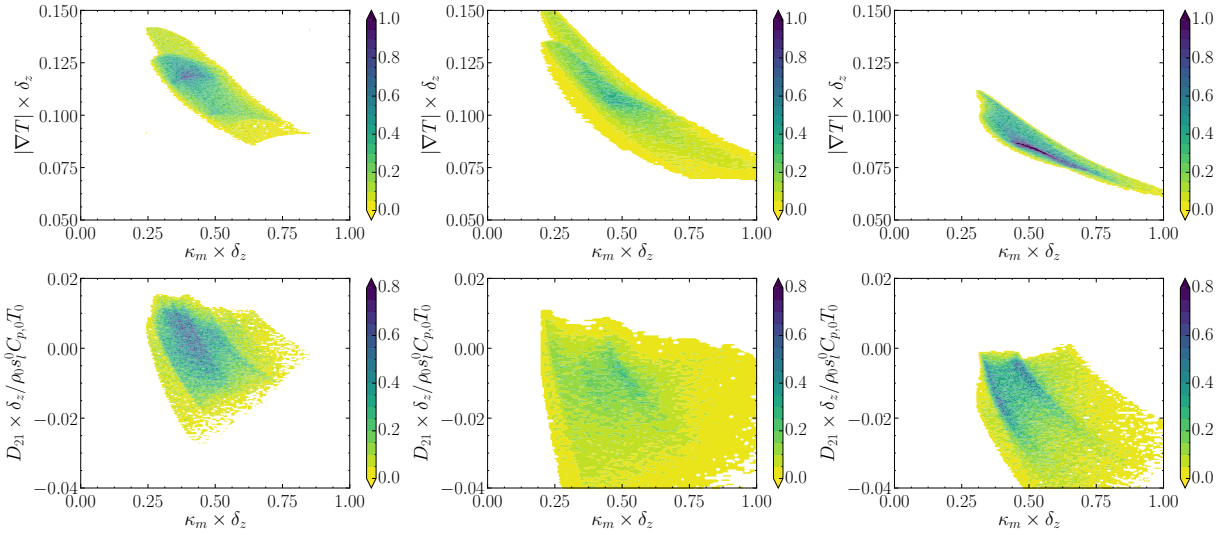

Figure 13: *(top)* $P(\kappa_m,\ |\nabla T|)$ and *(bottom)* $P(\kappa_m,\ D_{21})$ for $u'/s_l^0 = 9.0$, $\Gamma = \Gamma^i_{\mathrm{MIE}}$, $t/t_{sp} \approx 1.0$ and $T = 0.3$ using three different realisations of turbulence *(left to right)* Real. 1, 2, 3

5. Discussion and physical insights

The DNS results presented in this paper qualitatively capture the experimentally observed MIE transition, but it is necessary to identify and explain the physical mechanism which is responsible for this behaviour. The mean heat release rate conditional on the temperature (T) needs to be greater than the magnitude of the mean conditional thermal diffusion rate for successful ignition and self-sustained flame propagation to occur. The opposite is true for misfire or kernel quenching. However, the magnitude of the MIE is dependent on the competition between the overall heat release rate and heat transfer, which cannot be readily extracted from plots in Fig. 11 as it does not provide the number of samples corresponding to every value of T, and the volume integral of molecular dissipation rate $\nabla \cdot (\lambda \nabla \hat{T})$ is expected to vanish because of the divergence theorem (i.e. $\int_V \nabla \cdot (\lambda \nabla \hat{T})\, \mathrm{d}V = 0$). Thus, to explain the MIE transition, a scaling analysis, which is presented below, based on the physics highlighted in the next subsection has been carried out.

5.1. Governing physics

The flame surface area $\mathcal{A}$ increases with increasing turbulence intensity u'/s_l^0, which acts to increase the overall burning rate. Simultaneously, the turbulent (eddy) diffusivity also increases as it scales with u' ($D_t \sim u' l_t$). It has already been discussed that the competition between the overall chemical heat release and thermal diffusion governs the ignition/propagation success, and both the flame surface area and turbulent diffusivity affect these two governing mechanisms.

On one hand, as u'/s_l^0 increases, both the flame surface area and the turbulent diffusivity increase, however, the extent to which the flame surface area can increase is limited. The flame surface area growth

due to turbulence is limited due to e.g. flame-flame interaction, which leads to the bending effect outlined by previous experimental and numerical studies [58–63]. This bending effect in the variation of $\mathcal{A}_T/\mathcal{A}_p$ (where $\mathcal{A}_T$ and $\mathcal{A}_p$ are the turbulent and laminar flame areas respectively) as a function of u'/s_l^0 has indeed been found in this analysis (not shown here for brevity), which indicates that $\mathcal{A}_T/\mathcal{A}_p$ initially increases almost linearly for small values of u'/s_l^0, but for higher values, the flame surface area can be seen to taper off, before becoming nearly constant, and even decreasing slightly as u'/s_l^0 keeps increasing. By contrast, the turbulent diffusivity increases monotonically with increasing u'/s_l^0 for a given integral length scale.

On the other hand, the flame surface area to volume ratio (Σ') of the gas kernel plays a key role in the competition between the heat transfer rate and the chemical heat release, and the effects of the former become crucial for large surface to volume ratios. The value of Σ' decreases with increasing flame radius and thus the flame is more prone to quenching for smaller mean radii. However, as explained earlier, the increase in turbulent diffusivity with increasing turbulence intensity can be more rapid than the increase in flame surface area, especially at large values of u'/s_l^0. This effect is particularly important for small mean radii due to large values of Σ' that allow for the heat transfer to supersede the overall heat release leading to either a misfire or a flame quenching. To avoid this, the flame kernel needs to reach a mean critical radius R_{crit} [4–7] for self-sustained flame propagation to be obtained. In order to reduce the flame surface area to volume ratio to a value sufficient to support self-sustained flame propagation, for a given turbulence intensity, the flame kernel radius needs to be increased by depositing more energy. This critical kernel radius R_{crit} increases with u'/s_l^0 and is large for large turbulence intensities, such that Σ' assumes a value which compensates for the weaker increase in flame surface area compared to the rapid rise in turbulent diffusivity, to yield a balance between the overall heat release and heat transfer from the hot gas kernel. This is reflected by the rapid increase in MIE to obtain a successful ignition and/or propagation once a threshold turbulence intensity is reached, which has been demonstrated in Fig. 4. This observation can also be confirmed by the following scaling analysis.

5.2. Scaling analysis

The heat release must supersede the overall heat transfer rate from the kernel initiated by the local energy deposition to ensure that it propagates without the assistance of any external energy source. Thus, under the critical condition in the absence of any mean advection [25],

$$\int_V \dot{\omega}_T \, \mathrm{d}V \sim \rho_0 s_l^0 C_p (Y_{f,u} - Y_{f,b}) H_\phi \mathcal{A}_T \sim q_{\text{eff}} \mathcal{A}_p, \tag{6}$$

where $\dot{\omega}_T$ scales with $\rho_0 s_l^0 C_p (Y_{f,u} - Y_{f,b}) H_\phi \Sigma'$, $\mathcal{A}_T$ is the actual flamelet area, $\mathcal{A}_p$ the projected flame surface area and q_{eff} the effective diffusive thermal flux. It can be taken to scale as $q_{\text{eff}} \sim \rho_0 C_p (D + D_t)(T_{ad} - T_0)/R_{\text{crit}}$. Henceforth, it will be considered that $D_t \gg D$ because turbulent diffusion is expected

to be much stronger than the molecular diffusion rate. Upon using $C_p(T_{ad} - T_0) = H_\phi(Y_{f,u} - Y_{f,b})$ and $D_t \sim u' l_t$, one gets [25],

$$R_{\text{crit}} \sim \frac{u' l_t}{s_l^0(\mathcal{A}_T/\mathcal{A}_p)}, \tag{7}$$

where $\mathcal{A}_T/\mathcal{A}_p$ is the wrinkling factor Ξ which is often scaled using a power-law as $\Xi \sim (u'/l_t)^n$ [10, 64, 65] with $0 < n < 1$. Using this scaling, Eq. 7 can be further scaled as,

$$R_{\text{crit}} \sim \delta_z (l_t/\delta_z)(u'/s_l^0)^{1-n}. \tag{8}$$

As the MIE can be taken to scale with the energy required to raise the temperature of the mass of gas of radius R_{crit} from the unburned gas conditions to the adiabatic flame temperature (i.e. $E_{\text{ign}} \sim \rho_0(4/3\pi\delta_z^3)C_p(T_{ad} - T_0)$), the normalised MIE, Γ^p_{MIE}, can be taken to scale as,

$$\Gamma^p_{\text{MIE}} \sim (l_t/\delta_z)^3 (u'/s_l^0)^{3-3n}. \tag{9}$$

It is worthwhile to note that $l_t/\delta_z \sim \text{Re}_t^{3/4}\text{Ka}^{-0.5}$ is also dependant on the turbulent Reynolds and the Karlovitz numbers, but in the current analysis, the initial value of l_t/δ_z is kept constant. Although the turbulence intensity decays with time, the values of u'/s_l^0 and l_t/δ_z at the time of the successful propagation have not been found to change significantly from their initial values. For $u'/s_l^0 = 4.0$, the decrease is roughly 12% at $t/t_{sp} = 10.0$, for $u'/s_l^0 = 14.0$, the decrease is about 16% at $t/t_{sp} = 8.0$ (time at which the kernel leaves the domain) and for $u'/s_l^0 = 22.0$ the decrease is approximately 12% at $t/t_{sp} = 4.0$. Several previous analysis [58–63] indicated bending effect where the wrinkling factor Ξ increases almost linearly with u'/s_l^0 for small turbulence intensities (i.e. $n \approx 1.0$), whereas for large values of u'/s_l^0, the wrinkling factor Ξ becomes less sensitive to the change in u'/s_l^0 (i.e. $n < 1$). A value of $n \approx 1.0$ is consistent with $\Gamma^p_{\text{MIE}} \sim (u'/s_l^0)^{0.03}$ found for small turbulence intensities in Fig. 4. By contrast, a value of $n \approx 1/3$ for large values of u'/s_l^0 yields $\Gamma^p_{\text{MIE}} \sim (u'/s_l^0)^2$ as observed from Fig. 4. The wrinkling factor correlation was indeed proposed to be $\Xi \sim (u'/s_l^0)^{0.4}$ in previous analyses on turbulent flame speed [64, 65]. Further discussion on the bending phenomenon is beyond the scope of this analysis as is the parametrisation of the power-law exponent n (but a preliminary analysis reveals that the flame kernels in this dataset shows $n \approx 0.3$). However, the above scaling analysis and its apparent agreement with the current data (Γ^p_{MIE}) offers an alternative perspective for the transition in MIE.

6. Conclusions

The minimum ignition energy (MIE) of a stoichiometric methane-air mixture in homogeneous isotropic decaying turbulence has been numerically evaluated for a large range of initial turbulence intensities. A good qualitative agreement has been found with the available experimental results [8, 9, 11, 12], with the prediction of a transition in the MIE between low to moderate and large turbulence intensities. However, there are significant quantitative discrepancies in the MIE dependence on u'/s_l^0 between the experimental data by Shy and his co-workers [8, 9] and the present computational results, but much smaller ones between the DNS data and the experimental results of Cardin *et al.* [11, 12]. This variation in the quantitative agreement has been attributed to the different integral length scales, flow conditions (e.g. forced turbulence in [8, 9] as opposed to decaying turbulence in DNS and in [11, 12]) and ignition systems used in the experiments and the DNS. The fundamentally stochastic behaviour of the ignition has also been reproduced numerically by depositing an identical amount of energy to three statistically identical realisations of turbulence (u'/s_l^0 and l_t/δ_z) and measuring the probability of successful ignition/propagation. Furthermore, the energy distribution following its deposition was investigated and it was found that ignition was successful only if the ratio of the maximum value of mean magnitudes of chemical heat release and thermal diffusion rate conditioned on T was greater than unity at the end of the energy deposition. The stochastic behaviour of the ignition process was also attributed to the key role of the spatial fluctuations of local isotherms curvature. They affect the normal component of diffusion rate and thus the overall thermal diffusion rate leading to a misfire if it supersedes the heat release rate. Using a scaling analysis of the energy balance, a parametrisation of the MIE sufficient for self-sustained flame propagation following successful ignition is proposed as a function of the turbulence intensity. The proposed scaling matches the MIE dependence on the turbulence intensity found numerically, and the insights gained from the simulation data have been used to explain the physical mechanisms behind the transition in MIE requirements with increasing turbulence intensity. Finally, it is recognised that the single-step chemistry and the unity Lewis number assumptions used in this work preclude the analysis of the differential diffusion, thermodiffusive instabilities, low-temperature kinetics or gas ionisation effects on the ignition process and its influence on the MIE. However, the qualitative nature of the turbulence-chemistry interaction is not expected to change in the presence of detailed chemistry but some quantitative differences due to aforementioned effects may arise. These differences could affect the absolute energy levels or the kernel behaviour, although the MIE transition and dependence on turbulence intensity should remain qualitatively similar. Further investigation of these effects will form the basis of future investigations.

Acknowledgements

The authors are grateful to the British Council, EPSRC, Rocket (HPC facility at Newcastle University), Cirrus and ARCHER for financial and computational support respectively.

References

[1] C. Vázquez-Espí, A. Liñán, Fast, non-diffusive ignition of a gaseous reacting mixture subject to a point energy source, Combust. Theory Model. 5 (3) (2001) 485–498. doi:10.1088/1364-7830/5/3/313.

[2] C. Vázquez-Espí, A. Liñán, Thermal-diffusive ignition and flame initiation by a local energy source, Combust. Theory Model. 6 (2) (2002) 297–315. doi:10.1088/1364-7830/6/2/309.

[3] M. Champion, B. Deshaies, Spherical flame ignition: theory versus experiment for lean propane-air mixtures, Combust. Flame 65 (1986) 319–337.

[4] D. R. Ballal, A. H. Lefebvre, The influence of flow parameters on minimum ignition energy and quenching distance, Symp. Combust. 15 (1) (1975) 1473–1481. doi:10.1016/S0082-0784(75)80405-X.

[5] D. R. Ballal, A. H. Lefebvre, Ignition and flame quenching of flowing heterogeneous fuel-air mixtures, Combust. Flame 35 (1979) 155–168.

[6] D. R. Ballal, A. H. Lefebvre, A general model of spark ignition for gaseous and liquid fuel-air mixtures, Symp. Combust. 18 (1) (1981) 1737–1746. doi:10.1016/S0082-0784(81)80178-6.

[7] A. H. Lefebvre, D. R. Ballal, Gas turbine combustion: alternative fuels and emissions, 3rd Edition, CRC Press, 2010.

[8] C. Huang, S. S. Shy, C. C. Liu, Y. Yan, A transition on minimum ignition energy for lean turbulent methane combustion in flamelet and distributed regimes, Proc. Combust. Inst. 31 (1) (2007) 1401–1409. doi:10.1016/j.proci.2006.08.024.

[9] S. S. Shy, C. C. Liu, W. Shih, Ignition transition in turbulent premixed combustion, Combust. Flame 157 (2) (2010) 341–350. doi:10.1016/j.combustflame.2009.08.005.

[10] S. Chaudhuri, F. Wu, C. K. Law, Scaling of turbulent flame speed for expanding flames with Markstein diffusion considerations, Phys. Rev. E 88 (3) (2013) 033005. doi:10.1103/PhysRevE.88.033005.

[11] C. Cardin, B. Renou, G. Cabot, A. M. Boukhalfa, Experimental analysis of laser-induced spark ignition of lean turbulent premixed flames: New insight into ignition transition, Combust. Flame 160 (8) (2013) 1414–1427. doi:10.1016/j.combustflame.2013.02.026.

[12] C. Cardin, B. Renou, G. Cabot, A. M. Boukhalfa, Experimental analysis of laser-induced spark ignition of lean turbulent premixed flames, Comptes Rendus Mécanique 341 (1-2) (2013) 191–200. doi:10.1016/j.crme.2012.10.019.

[13] M. W. Peng, S. S. Shy, Y. W. Shiu, C. C. Liu, High pressure ignition kernel development and minimum ignition energy measurements in different regimes of premixed turbulent combustion, Combust. Flame 160 (9) (2013) 1755–1766. doi:10.1016/j.combustflame.2013.03.030.

[14] I. A. Mulla, S. R. Chakravarthy, N. Swaminathan, R. Balachandran, Evolution of flame-kernel in laser-induced spark ignited mixtures: A parametric study, Combust. Flame 164 (2016) 303–318. doi:10.1016/j.combustflame.2015.11.029.

[15] S. S. Shy, M. T. Nguyen, S.-Y. Huang, C.-C. Liu, Is turbulent facilitated ignition through differential diffusion independent of spark gap?, Combust. Flame 185 (2017) 1–3. doi:10.1016/j.combustflame.2017.06.022.

[16] S. S. Shy, Y. W. Shiu, L. J. Jiang, C. C. Liu, S. Minaev, Measurement and scaling of minimum ignition energy transition for spark ignition in intense isotropic turbulence from 1 to 5 atm, Proc. Combust. Inst. 36 (2) (2017) 1785–1791. doi:10.1016/j.proci.2016.08.049.

[17] L. J. Jiang, S. S. Shy, M. T. Nguyen, S. Y. Huang, D. W. Yu, Spark ignition probability and minimum ignition energy transition of the lean iso-octane/air mixture in premixed turbulent combustion, Combust. Flame 187 (2018) 87–95. doi:10.1016/j.combustflame.2017.09.006.

[18] A. Frendi, M. Sibulkin, Dependence of minimum ignition energy on ignition parameters, Combust. Sci. Technol. 73 (1-3) (1990) 395–413. doi:10.1080/00102209008951659.

[19] M. Thiele, S. Selle, U. Riedel, J. Warnatz, U. Maas, Numerical simulation of spark ignition including ionization, Proc. Combust. Inst. 28 (1) (2000) 1177–1185. doi:10.1016/S0082-0784(00)80328-8.

[20] M. Thiele, J. Warnatz, A. Dreizler, S. Lindenmaier, R. Schießl, U. Maas, A. Grant, P. Ewart, Spark ignited hydrogen/air

mixtures: Two dimensional detailed modeling and laser based diagnostics, Combust. Flame 128 (1-2) (2002) 74–87. doi:10.1016/S0010-2180(01)00333-9.

[21] M. Baum, T. Poinsot, Effects of mean flow on premixed flame ignition, Combust. Sci. Technol. 106 (1-3) (1995) 19–39. doi:10.1080/00102209508907765.

[22] T. Poinsot, S. Candel, A. Trouvé, Applications of direct numerical simulation to premixed turbulent combustion, Prog. Energy Combust. Sci. 21 (6) (1996) 531–576. doi:10.1016/0360-1285(95)00011-9.

[23] M. Thiele, J. Warnatz, U. Maas, Geometrical study of spark ignition in two dimensions, Combust. Theory Model. 4 (4) (2000) 413–434. doi:10.1088/1364-7830/4/4/303.

[24] C. F. Kaminski, J. Hult, M. Aldén, S. Lindenmaier, A. Dreizler, U. Maas, M. Baum, Spark ignition of turbulent methane/air mixtures revealed by time-resolved planar laser-induced fluorescence and direct numerical simulations, Proc. Combust. Inst. 28 (1) (2000) 399–405. doi:10.1016/S0082-0784(00)80236-2.

[25] M. Klein, N. Chakraborty, S. Cant, Effects of turbulence on self-sustained combustion in premixed flame kernels: A direct numerical dimulation (DNS) study, Flow, Turbul. Combust. 81 (4) (2008) 583–607. doi:10.1007/s10494-008-9149-z.

[26] D. Patel, N. Chakraborty, Effects of energy deposition characteristics on localised forced ignition of homogeneous mixtures, Int. J. Spray Combust. Dyn. 7 (2) (2015) 151–174. doi:10.1260/1756-8277.7.2.151.

[27] E. Mastorakos, Ignition of turbulent non-premixed flames, Prog. Energy Combust. Sci. 35 (1) (2009) 57–97. doi:10.1016/j.pecs.2008.07.002.

[28] E. Mastorakos, Forced ignition of turbulent spray flames, Proc. Combust. Inst. 36 (2) (2017) 2367–2383. doi:10.1016/j.proci.2016.08.044.

[29] C. Catlin, M. Fairweather, S. Ibrahim, Predictions of turbulent, premixed flame propagation in explosion tubes, Combust. Flame 102 (1-2) (1995) 115–128. doi:10.1016/0010-2180(94)00245-N.

[30] D. Patel, N. Chakraborty, Effects of fuel Lewis number on localised forced ignition of turbulent homogeneous mixtures: A numerical investigation, Int. J. Spray Combust. Dyn. 8 (3) (2016) 183–196. doi:10.1177/1756827716651579.

[31] N. Chakraborty, E. Mastorakos, Direct numerical simulations of localised forced ignition in turbulent mixing layers: The effects of mixture fraction and its gradient, Flow, Turbul. Combust. 80 (2) (2008) 155–186. doi:10.1007/s10494-007-9110-6.

[32] A. Neophytou, E. Mastorakos, S. Cant, DNS of spark ignition and edge flame propagation in turbulent droplet-laden mixing layers, Combust. Flame 157 (6) (2010) 1071–1086. doi:10.1016/j.combustflame.2010.01.019.

[33] A. P. Wandel, Influence of scalar dissipation on flame success in turbulent sprays with spark ignition, Combust. Flame 161 (10) (2014) 2579–2600. doi:10.1016/j.combustflame.2014.04.006.

[34] D. Patel, N. Chakraborty, Localised forced ignition of globally stoichiometric stratified mixtures: A numerical investigation, Combust. Theory Model. 18 (6) (2014) 627–651. doi:10.1080/13647830.2014.959456.

[35] N. Chakraborty, S. Cant, Unsteady effects of strain rate and curvature on turbulent premixed flames in an inflow-outflow configuration, Combust. Flame 137 (1-2) (2004) 129–147. doi:10.1016/j.combustflame.2004.01.007.

[36] N. Chakraborty, E. R. Hawkes, J. H. Chen, S. Cant, The effects of strain rate and curvature on surface density function transport in turbulent premixed methane-air and hydrogen-air flames: A comparative study, Combust. Flame 154 (1-2) (2008) 259–280. doi:10.1016/j.combustflame.2008.03.015.

[37] N. Peters, P. Terhoeven, J. H. Chen, T. Echekki, Statistics of flame displacement speeds from computations of 2-D unsteady methane-air flames, Symp. Combust. 27 (1) (1998) 833–839. doi:10.1016/S0082-0784(98)80479-7.

[38] N. Chakraborty, M. Klein, Influence of Lewis number on the surface density function transport in the thin reaction zone regime for turbulent premixed flames, Phys. Fluids 20 (6) (2008) 065102. doi:10.1063/1.2919129.

[39] N. Chakraborty, H. Kolla, R. Sankaran, E. R. Hawkes, J. H. Chen, N. Swaminathan, Determination of three-dimensional quantities related to scalar dissipation rate and its transport from two-dimensional measurements: Direct numerical

simulation based validation, Proc. Combust. Inst. 34 (1) (2013) 1151–1162. doi:10.1016/j.proci.2012.06.040.

[40] A. Haghiri, M. Talei, M. J. Brear, E. R. Hawkes, Sound generation by turbulent premixed flames, J. Fluid Mech. 843 (2018) 29–52. doi:10.1017/jfm.2018.115.

[41] L. He, Critical conditions for spherical flame initiation in mixtures with high Lewis numbers, Combust. Theory Model. 4 (2) (2000) 159–172. doi:10.1088/1364-7830/4/2/305.

[42] E. Mastorakos, T. A. Baritaud, T. Poinsot, Numerical simulations of autoignition in turbulent mixing flows, Combust. Flame 109 (1-2) (1997) 198–223. doi:10.1016/S0010-2180(96)00149-6.

[43] N. Chakraborty, Comparison of displacement speed statistics of turbulent premixed flames in the regimes representing combustion in corrugated flamelets and thin reaction zones, Phys. Fluids 19 (10) (2007) 1–20. doi:10.1063/1.2784947.

[44] A. P. Wandel, N. Chakraborty, E. Mastorakos, Direct numerical simulations of turbulent flame expansion in fine sprays, Proc. Combust. Inst. 32 II (2009) 2283–2290. doi:10.1016/j.proci.2008.06.102.

[45] J. Ray, H. N. Najm, R. B. Mccoy, Ignition front structure in a methane-air jet, 2nd Jt. Meet. US Sect. Combust. Inst. (150).

[46] R. Hilbert, D. Thevenin, Dns of multi-brachial structures with detailed chemistry and transport, in: Proceedings of the 9th International Conference on Numerical Combustion, Paper, no. 064, Sorrento, Italy, 2002.

[47] D. R. Ballal, A. H. Lefebvre, Spark ignition of turbulent flowing gases, in: 15th Aerosp. Sci. Meet., Vol. 155, American Institute of Aeronautics and Astronautics, Reston, Virigina, 1977, pp. 129–155. doi:10.2514/6.1977-185.

[48] N. Chakraborty, E. Mastorakos, S. Cant, Effects of turbulence on spark ignition in inhomogeneous mixtures: A direct numerical simulation (DNS) study, Combust. Sci. Technol. 179 (1-2) (2007) 293–317. doi:10.1080/00102200600809555.

[49] K. Jenkins, R. Cant, Direct numerical simulation of turbulent flame kernels, in: D. Knight, L. Sakell (Eds.), Recent Advances in DNS and LES: Proceedings of the Second AFOSR Conference, Rutgers - The State University of New Jersey, New Brunswick, USA, Kluwer, Dordrecht, 1999, pp. 191–202.

[50] J. C. Sutherland, C. A. Kennedy, Improved boundary conditions for viscous, reacting, compressible flows, J. Comput. Phys. 191 (2) (2003) 502–524. doi:10.1016/S0021-9991(03)00328-0.

[51] A. Wray, Minimal storage time advancement schemes for spectral methods, NASA Ames Research Center, California (1990).

[52] R. S. Rogallo, Numerical experiments in homogeneous turbulence, Tech. rep., NASA Ames (1981).

[53] G. K. Batchelor, A. A. Townsend, The nature of turbulent motion at large wave-numbers, Proc. R. Soc. A Math. Phys. Eng. Sci. 199 (1057) (1949) 238–255. doi:10.1098/rspa.1949.0136.

[54] C. Pera, S. Chevillard, J. Reveillon, Effects of residual burnt gas heterogeneity on early flame propagation and on cyclic variability in spark-ignited engines, Combust. Flame 160 (6) (2013) 1020–1032. doi:10.1016/j.combustflame.2013.01.009.

[55] R. Yu, X.-S. Bai, Direct numerical simulation of lean hydrogen/air auto-ignition in a constant volume enclosure, Combust. Flame 160 (9) (2013) 1706–1716. doi:10.1016/j.combustflame.2013.03.025.

[56] H. G. Im, J. H. Chen, C. K. Law, Igintion of hydrogen-air mixing layer in turbulent flows, Twenty-Seventh Symp. Combust. (1998) 1047–1056.

[57] M. Klein, N. Chakraborty, K. Jenkins, S. Cant, Effects of initial radius on the propagation of premixed flame kernels in a turbulent environment, Phys. Fluids 18 (5) (2006) 055102. doi:10.1063/1.2196092.

[58] R. G. Abdel-Gayed, D. Bradley, Dependence of turbulent burning velocity on turbulent Reynolds number and ratio of laminar burning velocity to R.M.S. turbulent velocity, Symp. Combust. 16 (1) (1977) 1725–1735. doi:10.1016/S0082-0784(77)80450-5.

[59] R. G. Abdel-Gayed, K. J. Al-Khishali, D. Bradley, Turbulent burning velocities and flame straining in explosions, Proc. R. Soc. A Math. Phys. Eng. Sci. 391 (1801) (1984) 393–414. doi:10.1098/rspa.1984.0019.

[60] D. Bradley, How fast can we burn?, Symp. Combust. 24 (1) (1992) 247–262. doi:10.1016/S0082-0784(06)80034-2.

[61] D. Bradley, Problems of predicting turbulent burning rates, Combust. Theory Model. 6 (2) (2002) 361–382. doi:10.1088/1364-7830/6/2/312.

[62] K. N. C. Bray, Studies of the turbulent burning velocity, Proc. R. Soc. A Math. Phys. Eng. Sci. 431 (1990) 315–335. doi:10.1098/rspa.1990.0133.

[63] G. Nivarti, S. Cant, Direct numerical simulation of the bending effect in turbulent premixed flames, Proc. Combust. Inst. 36 (2) (2017) 1903–1910. doi:10.1016/j.proci.2016.07.076.

[64] S. P. Reddy Muppala, N. K. Aluri, F. Dinkelacker, A. Leipertz, Development of an algebraic reaction rate closure for the numerical calculation of turbulent premixed methane, ethylene, and propane/air flames for pressures up to 1.0 MPa, Combust. Flame 140 (4) (2005) 257–266. doi:10.1016/j.combustflame.2004.11.005.

[65] H. Kobayashi, H. Kawazoe, Flame instability effects on the smallest wrinkling scale and burning velocity of high-pressure turbulent premixed flames, Proc. Combust. Inst. 28 (1) (2000) 375–382. doi:10.1016/S0082-0784(00)80233-7.